

# NASA CONTRACTOR REPORT

CR-61158

November 28, 1966

CR-61158

## A COMPARISON OF FPS-16 AND GMD-1 MEASUREMENTS AND METHODS FOR PROCESSING WIND DATA

Final Report, Phase II

ANALYSIS OF TIME VARIABILITY OF ATMOSPHERIC PARAMETERS

By E. F. Danielsen and R. T. Duquet

Prepared under Contract No. NAS 8-11145 by  
PENNSYLVANIA STATE UNIVERSITY

FACILITY FORM 602

**N67-11984**  
ACCESSION NUMBER

66  
(PAGES)

CR-61158  
(NASA CR OR TMX OR AD NUMBER)

\_\_\_\_\_  
(THRU)

1  
(CODE)

13  
(CATEGORY)

GPO PRICE \$ \_\_\_\_\_

CFSTI PRICE(S) \$ \_\_\_\_\_

Hard copy (HC) 3.00

Microfiche (MF) 1.50

ff 653 July 65

For

GEORGE C. MARSHALL SPACE FLIGHT CENTER  
Huntsville, Alabama

November 28, 1966

CR-61158

A COMPARISON OF FPS-16 AND GMD-1 MEASUREMENTS AND  
METHODS FOR PROCESSING WIND DATA

Final Report, Phase II  
ANALYSIS OF TIME VARIABILITY OF  
ATMOSPHERIC PARAMETERS

By

E. F. Danielsen and R. T. Duquet\*

Prepared under Contract No. NAS 8-11145 by

PENNSYLVANIA STATE UNIVERSITY

\* Associate Professors of Meteorology

**Distribution of this report is provided in the interest of  
information exchange. Responsibility for the contents  
resides in the author or organization that prepared it.**

GEORGE C. MARSHALL SPACE FLIGHT CENTER

TABLE OF CONTENTS

	Page
LIST OF FIGURES . . . . .	v
ABSTRACT . . . . .	
SECTION 1. INTRODUCTION . . . . .	1
SECTION 2. OBJECTIVES . . . . .	2
SECTION 3. DEFINITION OF A STANDARD . . . . .	2
3A. FPS-16 Measurements . . . . .	2
3B. Method of Processing FPS-16 Data. . . . .	3
3C. Examples of Winds and Balloon Ascent Rates. . . . .	5
SECTION 4. COMPARISON OF FPS-16 AND GMD-1 MEASUREMENTS . . . . .	6
SECTION 5. GMD-1 DATA PROCESSING . . . . .	7
5A. GMD-1 Measurements and Data Reduction . . . . .	7
5B. Computational Methods . . . . .	9
SECTION 6. COMPARISON OF FPS-16 AND GMD-1 ASCENT RATES AND WINDS . . . . .	11
6A. Ascent Rates . . . . .	11
6B. Wind Profiles and Hodographs . . . . .	12
1. Ascent of February 7, 1964 . . . . .	13
2. Ascent of February 20, 1964 . . . . .	14
3. Third Ascent of March 7, 1964 . . . . .	15
6C. Difficulties Associated with Very Low Elevation Angles . . . . .	15
SECTION 7. DETERMINATION OF ERRORS IN GMD ELEVATION ANGLES. . . . .	16
SECTION 8. GMD-1 DATA PROCESSING FOR VERY LOW ELEVATION ANGLES . . . . .	18
SECTION 9. WIND COMPARISONS AT VERY LOW ELEVATION ANGLES . . . . .	20
9A. First Ascent of March 7, 1964 . . . . .	20
9B. Second Ascent of March 7, 1964 . . . . .	21
SECTION 10. EVIDENCE OF GRAVITY AND GRAVITY-INERTIAL WAVES . . . . .	22

TABLE OF CONTENTS (CONT'D)

	Page
SECTION 11. CONCLUSIONS. . . . .	23
APPENDIX COMPUTER PROGRAMS. . . . .	25
REFERENCES . . . . .	37

## LIST OF FIGURES

	Page Number
Figure 1: Example of FPS-16 elevation angles, February 7, 1964	2a
Figure 2: Example of FPS-16 elevation angles, February 20, 1964	2a
Figure 3: FPS-16 wind speeds and ascent rates from 40 min 10 sec to 42 min 40 sec after release on February 7, 1964	4a
Figure 4: FPS-16 wind speeds and ascent rates from 42 min 10 sec to 45 min 10 sec, February 7, 1964	4a
Figure 5: Power Spectra of FPS-16 winds, February 7, 1964	5a
Figure 6: Comparison of GMD and FPS-16 elevation angles 38 min to 40 min 10 sec after release, February 7, 1964	6a
Figure 7: Comparison of GMD and FPS-16 elevation angles 40 min 10 sec to 42 min 40 sec after release, February 7, 1964	6b
Figure 8: Comparison of GMD and FPS-16 elevation angles 42 min 10 sec to 45 min 10 sec after release, February 7, 1964	6c
Figure 9: Balloon's ascent rates, February 7 and February 20, 1964	10a
Figure 10: Wind speed and temperature profiles, February 7, 1964	12a
Figure 11: FPS-16 wind velocity hodograph, February 7, 1964	12b
Figure 12: GMD-1 hodograph, February 7, 1964	12b
Figure 13: Wind speed and temperature profiles, February 20, 1964	13a
Figure 14: FPS-16 wind velocity hodograph, February 20, 1964	13b
Figure 15: GMD-1 hodograph, February 20, 1964	13b
Figure 16: Wind speed and temperature profile for 3rd ascent of March 7, 1964, (1659Z)	14a
Figure 17: FPS-16 hodograph for 3rd ascent of March 7, 1964	14b
Figure 18: GMD-1 hodograph for 3rd ascent of March 7, 1964	14b
Figure 19: Wind speed and temperature profile for 1st ascent, March 7, 1964 (0043Z)	15a
Figure 20: Errors in GMD elevation angles, February 7, 1964	16a
Figure 21: GMD and parallax adjusted FPS-16 elevation angles, February 20, 1964	17a
Figure 22: GMD and parallax adjusted FPS-16 elevation angles plus fourth order polynomial fit, 1st ascent of March 7, 1964, (0043Z)	17a

LIST OF FIGURES (CONT'D)

	Page Number
Figure 23: Winds based on polynomial fit to elevation angles, February 20, 1964	19a
Figure 24: Wind speed and temperature profiles for 1st ascent, March 7, 1964	20a
Figure 25: FPS-16 hodograph, 1st ascent, March 7, 1964	20b
Figure 26: GMD-1 hodograph, 1st ascent, March 7, 1964	20b
Figure 27: Wind speed and temperature profiles for 2nd ascent, March 7, 1964, (1107Z)	20c
Figure 28: FPS-16 hodograph, 2nd ascent, March 7, 1964	20d
Figure 29: GMD-1 hodograph, 2nd ascent, March 7, 1964	20d

ABSTRACT

11984

A machine method for computing winds from GMD-1 tracking and radiosonde data is developed and tested. The test includes a direct comparison of balloon ascent rates, horizontal wind speeds and directions with those computed from precision FPS-16 radar tracking data. In each of five cases tested, the GMD and radar measurements were made simultaneously by tracking the same effective target, i.e., a radiosonde transmitter and the chaff filled balloon which carried it aloft.

The method accurately reproduces the macroscale and mesoscale features of the wind speed profiles and vector hodographs when the elevation angles are greater than ten degrees. At lower elevation angles, long period, large magnitude errors in elevation angles produce errors in the winds which swamp the mesoscale features and distorted even the macroscale features. To recover reasonably accurate mean winds low order orthogonal polynomials are fitted to the measured elevation angles. The number of observations fitted by the polynomials is determined by applying a curvature criterion to the GMD-1 winds

The winds computed from the FPS-16 measurements contain, between the earth's surface and the maximum altitude reached by the radiosonde balloon, many oscillations in wind speed and direction. The hodographs suggest that the velocities can be decomposed into a mean wind vector and a perturbation vector which rotates cyclonically or anticyclonically with height. In the stratosphere, anticyclonic rotation predominates. The perturbation vectors have magnitudes ranging from 0.5 to 10 m/sec and rotate through  $2\pi$  radians in 0.5 to 3 km. The source of the perturbations remains unsolved but the properties of the vector wind and temperature perturbations are consistent with those of both inertial-gravity and shear-gravity.

*Author*

## SECTION 1. INTRODUCTION

The vertical profiles of the horizontal winds computed from precision radar tracking data, and from radar-sonde theodolite data, are complicated by numerous variations in both wind speed and direction (Barbe (1958), Scoggins (1965), and Sawyer (1960)). Many of the variations are oscillatory with vertical wave lengths less than 3 km. The combination of large magnitudes (1 - 5 m/sec) and small vertical wave lengths produces large velocity shears which are significant to the meteorologist and to the designers and engineers of aerospace vehicles.

The observation, identification and future prediction of these meso- and microscale oscillations is currently limited by the scarcity of precision radar installations. It would be a definite advantage if the oscillations could be accurately measured by the rawinsonde instruments. If the present rawin network is not sufficiently dense to resolve the horizontal distribution of the oscillations, the frequency of radiosonde ascents can be increased to provide a denser space-time network.

Measurements of azimuth and elevation angles must also be made at a higher than normal frequency by the GMD-1 or GMD-2 tracking equipment during each balloon's ascent. The current rate of one measurement per minute provides enough data to resolve only the larger of the mesoscale oscillations. Even this capability is destroyed by the crude methods and assumptions used in the conventional hand processing of the GMD data to compute the winds. Since the GMD equipment can be set to read azimuth and elevation angles ten times per minute and the data can be accurately processed by machines, resolution of the meso-scale and some of the microscale oscillations might be possible.

A special observational program designed to make this test was conducted in the southeastern United States during February 1964. The program was sponsored by the Aerospace Environment Division, NASA - Marshall Space Flight Center, with the cooperation of the U.S. Weather Bureau, the Air Force and Navy. At all regular radiosonde stations in the network, ascents were made every three hours. At Huntsville, Alabama, and at the Mississippi Test Site the ascents were made every ninety minutes. At all stations the GMD tracking equipment was set to record at its maximum rate. Also, care was taken to assure uniformity in the radiosonde base line checks.

All the data including the thermodynamic and tracking



measurements were read at Huntsville and recorded on tape for machine processing. The data processing has been a formidable task principally because of errors in the GMD measurements of elevation angles. In this report, the errors and the limitations they impose on wind computations are determined and machine methods for processing the data are evaluated.

## SECTION 2. OBJECTIVES

This study was undertaken to develop for the MSFC-NASA Project an objective method or methods of computing winds from GMD-1 data. Accuracy in both the mean wind and the deviations from the mean was desired. Clearly this would require a standard for distinguishing between real deviations and those resulting from errors in the data. Winds computed from precision radar tracking of a radiosonde balloon could serve as the standard if the radar and the GMD were simultaneously tracking the same target.

The Inter-Range Instrumentation Group-Meteorological Working Group has conducted experiments of this type using the FPS-16 radar, developed for rocket tracking, and a GMD-2 with a GMD-1 capability. Metallic chaff inside the balloon provided the target for the radar while the GMD tracked the radiosonde transmitter attached to the balloon. Slant range, azimuth and elevation angles were measured by the GMD-2 at the maximum rate of ten times per minute, the same rate as that used in the MSFC-NASA Project. Temperature and relative humidity were also measured alternately as a function of pressure (conventional baroswitching). Therefore a complete set of GMD-2 or GMD-1 measurements were available.

The authors were fortunate to receive five complete sets of tracking data from the IRIG/MWG. These data, all from Pt. Mugu, California, provide the basis for the study. In keeping with the desire to derive a data reduction method for the MSFC-NASA Project the study is concerned with the FPS-16 and the GMD-1 measurements.

## SECTION 3. DEFINITION OF A STANDARD

### 3A. FPS-16 Measurements

Every one tenth of a second the FPS-16 radar measures and records slant range to the nearest yard, azimuth and elevation angles to the nearest one thousandth of a degree. The accuracy

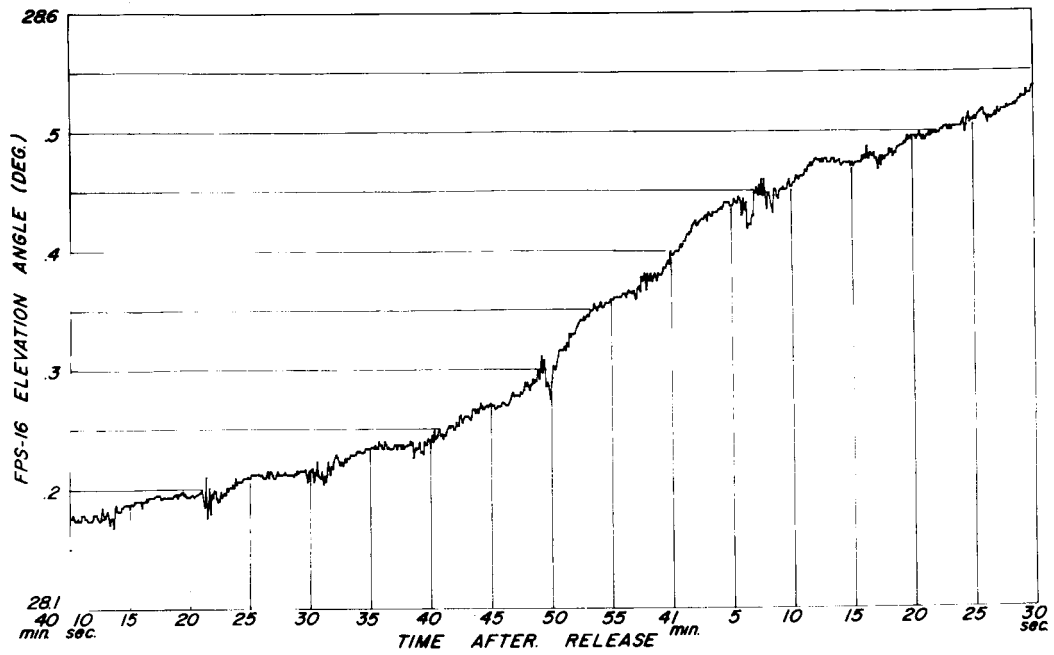


Figure 1: Example of FPS-16 elevation angles, February 7, 1964

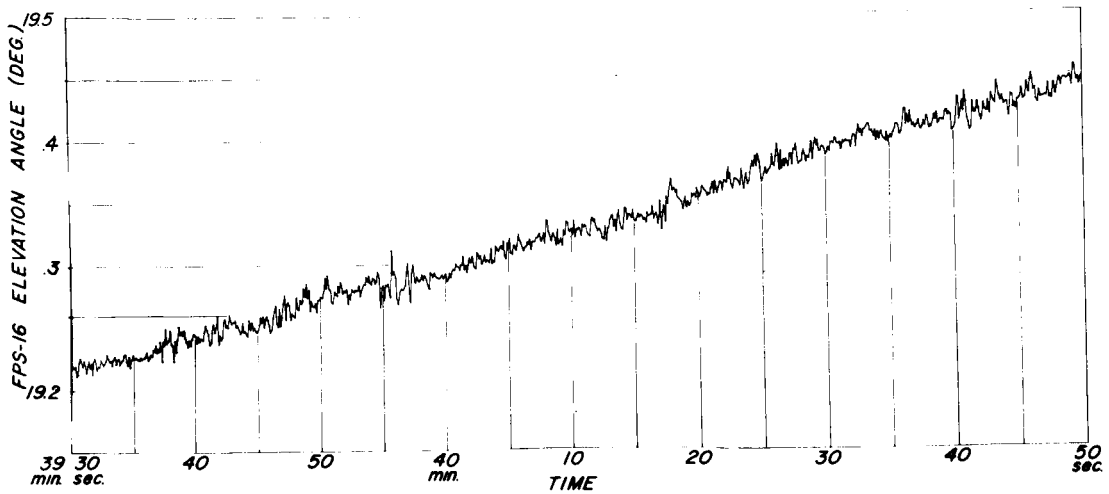


Figure 2: Example of FPS-16 elevation angles, February 20, 1964

of these measurements has been reviewed by Scoggins (1963) who accepts the values quoted by Sanderlin of an RMS accuracy of 5 yards in slant range and 0.01 degrees in azimuth and elevation angles.

Evidence of random and periodic errors in the elevation angles are shown in Figure 1 taken from a small segment of the data obtained during the ascent of February 7, 1964. The abscissa, which represents time after release, was divided into units of 5 sec beginning 40 min and 10 sec after release. The expanded ordinate scale, which spans only 0.5 deg, permitted accurate plotting to 0.001 deg. The observations were plotted as recorded every 0.1 sec. It is clear by inspection that the elevation angles contained periodic oscillations superimposed on a general increase. The period of the oscillations varied between 9 and 10 sec. Superimposed on these were high frequency random deviations, approximately 0.002 to 0.003 deg in magnitude. Large spurious deviations, 0.01 to 0.03 deg in magnitude, are also evident every 9 or 10 sec., i.e., at the same period as the above mentioned oscillations. These large errors, which appear to have been correlated with positive curvatures in the trace, must obviously be eliminated along with the smaller random deviations. It seemed desirable however to preserve the periodic oscillations to determine the magnitude of the speed oscillations they produce.

A second example taken from the ascent of February 20 is presented in Figure 2. In this case, the elevation angle was lower and was actually decreasing quite rapidly with time. To hold the entire trend on one diagram a uniform drop in elevation angle of 0.02 deg per sec was removed from the data. This produced an apparent increase in elevation angle. Figure 2 is consistently noisier than Figure 1. Evidence of periodic oscillations can only be detected by sighting down the curve. Superimposed on the gradual trend were frequent random fluctuations of approximately 0.01 deg with occasional fluctuations of 0.03 deg. Generally speaking, the errors throughout this ascent were greater than those of the 7th and the amplitude of the errors increased as the elevation angles decreased.

### 3B. Method of Processing FPS-16 Data

After examining several graphs of this type, it was decided that a relatively simple method of processing the FPS-16 data would provide the desired standard. To remove the high frequency oscillations without introducing spurious frequencies, the

arithmetic mean of every 10 consecutive non-overlapping points was computed. This generated 1 sec average values at intervals of 1 sec. Winds were then obtained by centered differencing.

Since winds were computed from azimuth angles and the distance of the balloon from the FPS-16 (measured on a curved earth), one might expect the resulting winds to differ, if

- (1) the distance was computed from the averaged values of range and elevation angle, or
- (2) the distances were first computed from the raw data and then averaged.

A test was conducted to compare the results of both methods. Differences in the computed winds were insignificant and therefore the second method was arbitrarily selected.

All calculations were made by a computer using the actual observations of slant range and angles. The height ( $z$ ) above the observing radar and distance over a curved earth ( $D$ ) were obtained from the following formulae:

$$1. \quad z = R \left[ \left( 1 + \frac{2r}{R} \sin \epsilon + \left( \frac{r}{R} \right)^2 \right)^{1/2} - 1 \right]$$

$$2. \quad D = R\theta = R \left[ \cos^{-1} \left( \frac{\cos \epsilon}{1 + \frac{z}{R}} \right) - \epsilon \right]$$

where  $R$  is the earth's radius,  $r$  is the slant range,  $\epsilon$  is the elevation angle and  $\theta$  is the angle between radii from the center of the earth to the radar and to the balloon.

The vertical and horizontal velocities of the balloon were computed for the  $i$ th point by finite differencing between the heights, times and horizontal positions at points  $i+1$  and  $i-1$ . This provided 2 sec average velocities of the balloon at a 1 sec interval. To determine the horizontal velocity of the air, the velocities of the balloon relative to the air must be removed. The relative velocities were expected to be oscillatory with periods of the order of 5 to 15 sec. Therefore 10, 20 and 40 sec average velocities were also computed by centered differencing and compared to the 2 sec average velocities. As before, the position coordinates were averaged without overlapping the data points but each average was now derived from 50, 100 and 200 consecutive points.

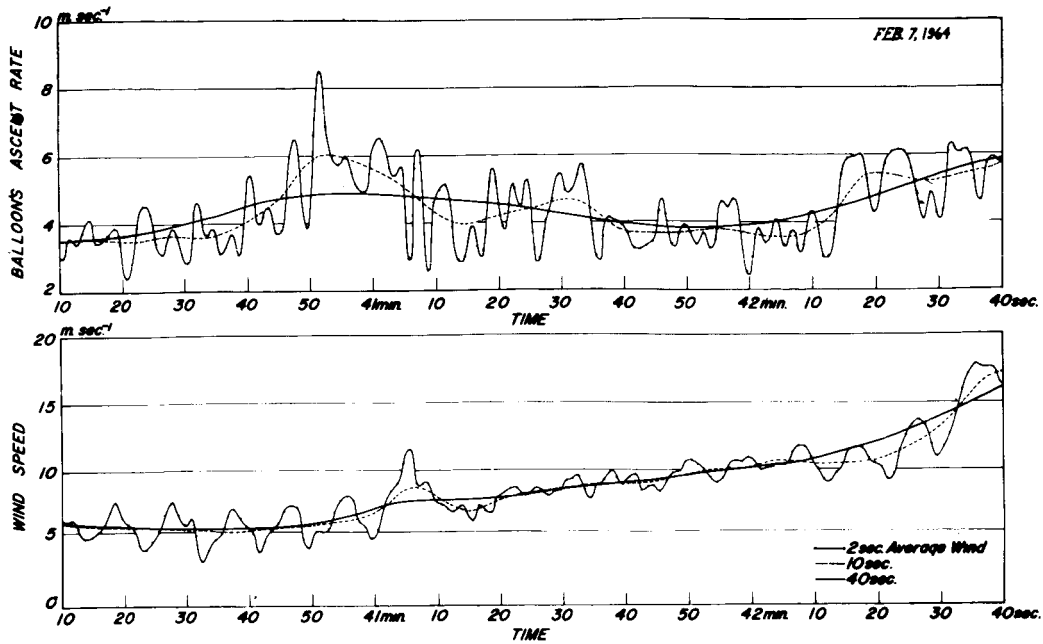


Figure 3: FPS-16 wind speeds and ascent rates from 40 min 10 sec to 42 min 40 sec after release on February 7, 1964

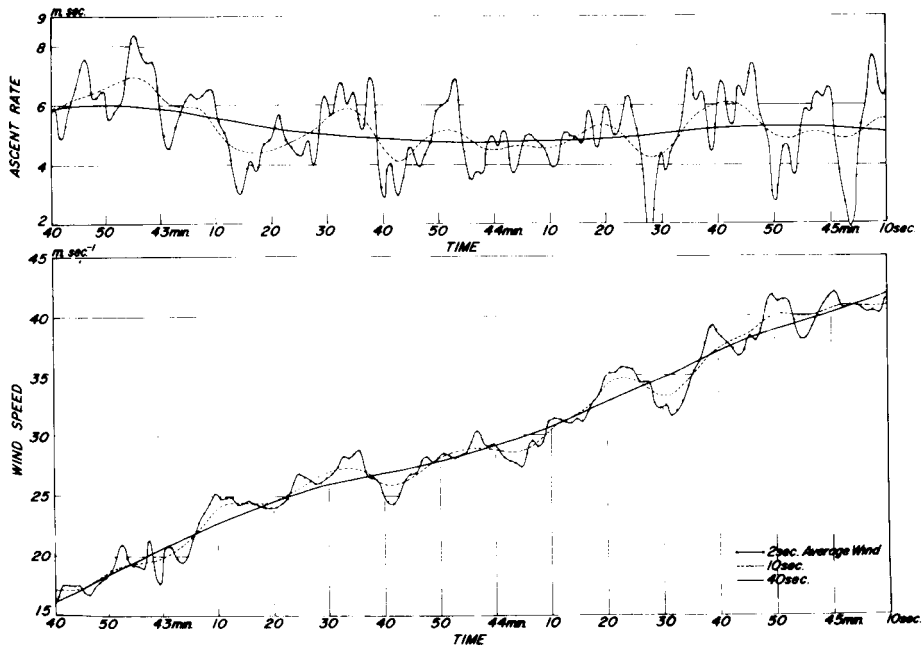


Figure 4: FPS-16 wind speeds and ascent rates from 42 min 10 sec to 45 min 10 sec, February 7, 1964

### 3C. Examples of Winds and Balloon Ascent Rates

Examples of the velocities computed by the above methods from the FPS-16 data are presented in Figures 3 and 4. Consecutive in time, they represent a small portion of the February 7 ascent. In both figures, the upper graph depicts the ascent rate of the balloon, the lower graph delineates the horizontal speed of the balloon. The latter, with reservations, has been labeled "wind speed". Figure 3 begins 40 min 10 sec after release, i.e., the same time as Figure 1. The periodic oscillations which were evident in the elevation angles of Figure 1 are clearly evident in the 2 sec average "wind speeds" of Figure 3. Oscillations of  $\pm 2$  m/sec with a period of about 9 sec characterize the first minute. During this time, the 10 sec average speeds (dashed line) and the 40 sec average speeds (heavy line) remained almost constant even though the elevation angle increased (Figure 1). This implies an increase in the average ascent rate of the balloon. The upper graph confirms the increase from 3.5 to 6 m/sec for the 10 sec average and 3.5 to 5 m/sec for the 40 sec average.

It is interesting to note that the oscillations in the 2 sec averages about the 40 sec averages are approximately  $\pm 2$  m/sec for both the vertical and horizontal components. Symmetry in the magnitude of the oscillations would be expected if they represent the balloons motion relative to the air. Also, although it is not regular, there is approximately a  $\pi/2$  phase shift between the respective components. The magnitudes, periods and phase shifts suggest they are produced by the balloon. For a discussion of the oscillations produced by ascending spherical balloons the reader is referred to a paper by Scoggins (1965).

If the assumption is correct that the high frequency oscillations are caused by accelerations of the balloon relative to the air then they are effectively removed by the 40 sec averages and the latter are a measure of the wind speed. If, on the other hand, the oscillations are real wind variations, they can only be treated statistically. Therefore, in all subsequent examples the 40 sec average winds computed from the FPS-16 data shall be considered as the standard for comparing the GMD winds. One might get the impression from Figures 3 and 4 that the 40 sec average oversmooths the data. This impression is due to the extended time scale. For an average ascent rate of 5 m/sec the complete abscissa represents a height interval of only  $3/4$  km. Despite the smooth appearance of the 40 sec average curves

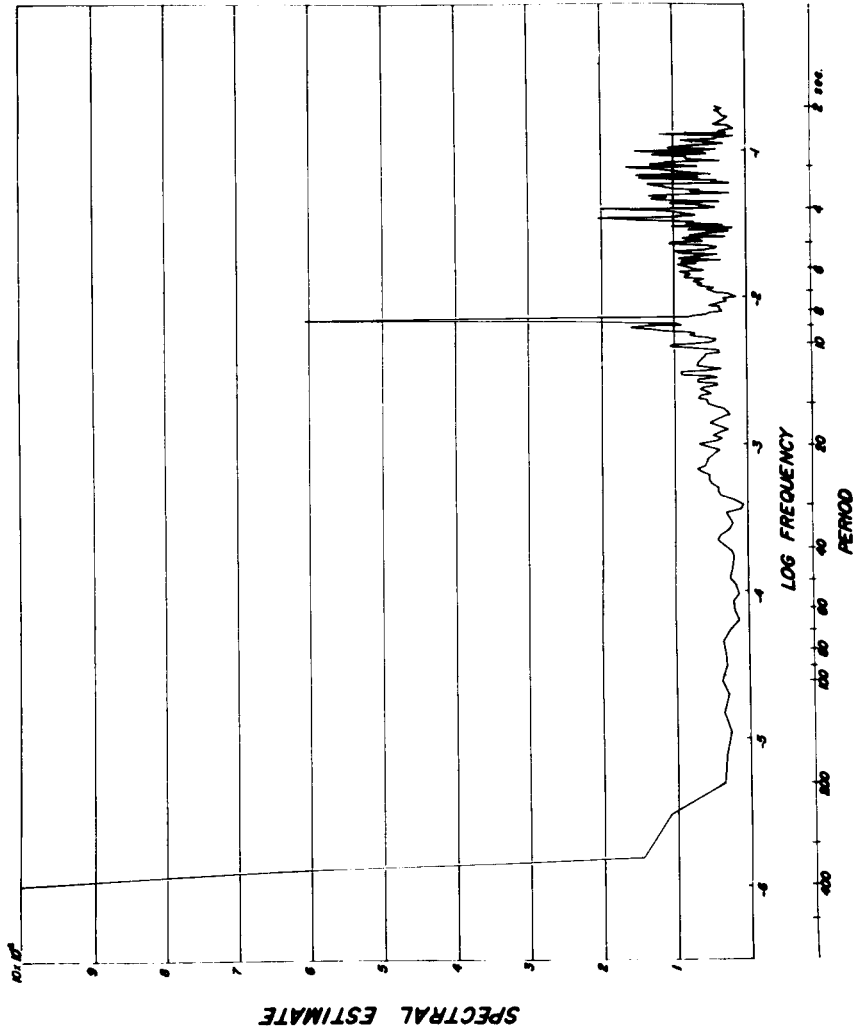


Figure 5: Power Spectra of FPS-16 winds, February 7, 1964

the complete profiles of wind speed vs height, hodographs and ascent rates, to be presented, contain an amazing complexity.

Additional support for the use of a 30 or 40 sec average as a standard can be derived from the power spectrum of the February 7, FPS-16 winds. The time series of the 2 sec average wind speeds (4977 values) were analyzed for 100 and 500 lags. The spectrum of the latter is shown in Figure 5. Long term trends were not removed from the original data. The ordinate is the product of the autocovariance and the lag divided by the standard deviation of the series. An outstanding feature is the spectral peak at 9 sec. This period, evident in the small sample of Figures 3 and 4, was predominant throughout the ascent. Again this suggests a natural period of the balloon. The power is a minimum between periods of 30 and 60 sec and remains relatively low up to 200 sec. The minimum implies that the averaging period could be increased to 200 sec which is equivalent to averaging over a vertical distance of 1 km. As will be shown, this would resolve the macroscale or synoptic scale features of the wind but would obscure the mesoscale features which presently concern us.

The power spectrum of the 2 sec average wind speeds was also computed from the February 20th winds. It resembled the spectrum shown in Figure 5 for all periods greater than 20 sec but it contained much more power at smaller periods. Large peaks in the power at 14 and 8 sec are attributed to the balloon while the power at periods less than 5 sec is attributed to the noise in the original data.

#### SECTION 4. COMPARISON OF FPS-16 AND GMD-1 MEASUREMENTS

Measurements of elevation angles contain the most troublesome errors in the GMD tracking system. An RMS error of 0.05 deg is commonly accepted for both the GMD-1 and GMD-2 measurements of azimuth and elevation angles. This is five times the FPS-16 error discussed earlier. However, in wind computations the RMS error may be a necessary but not sufficient criterion if the errors are occasionally large and somewhat organized rather than random. Errors of this type are evident in the GMD curves presented in Figures 6,7 and 8. These figures are consecutive in time and Figures 7 and 8 correspond respectively to Figures 3 and 4.

In Figures 6-8, the GMD elevation angles can be compared directly to the FPS-16 measurement, made at the same time from the same target. Only every other FPS-16 measurement was plotted



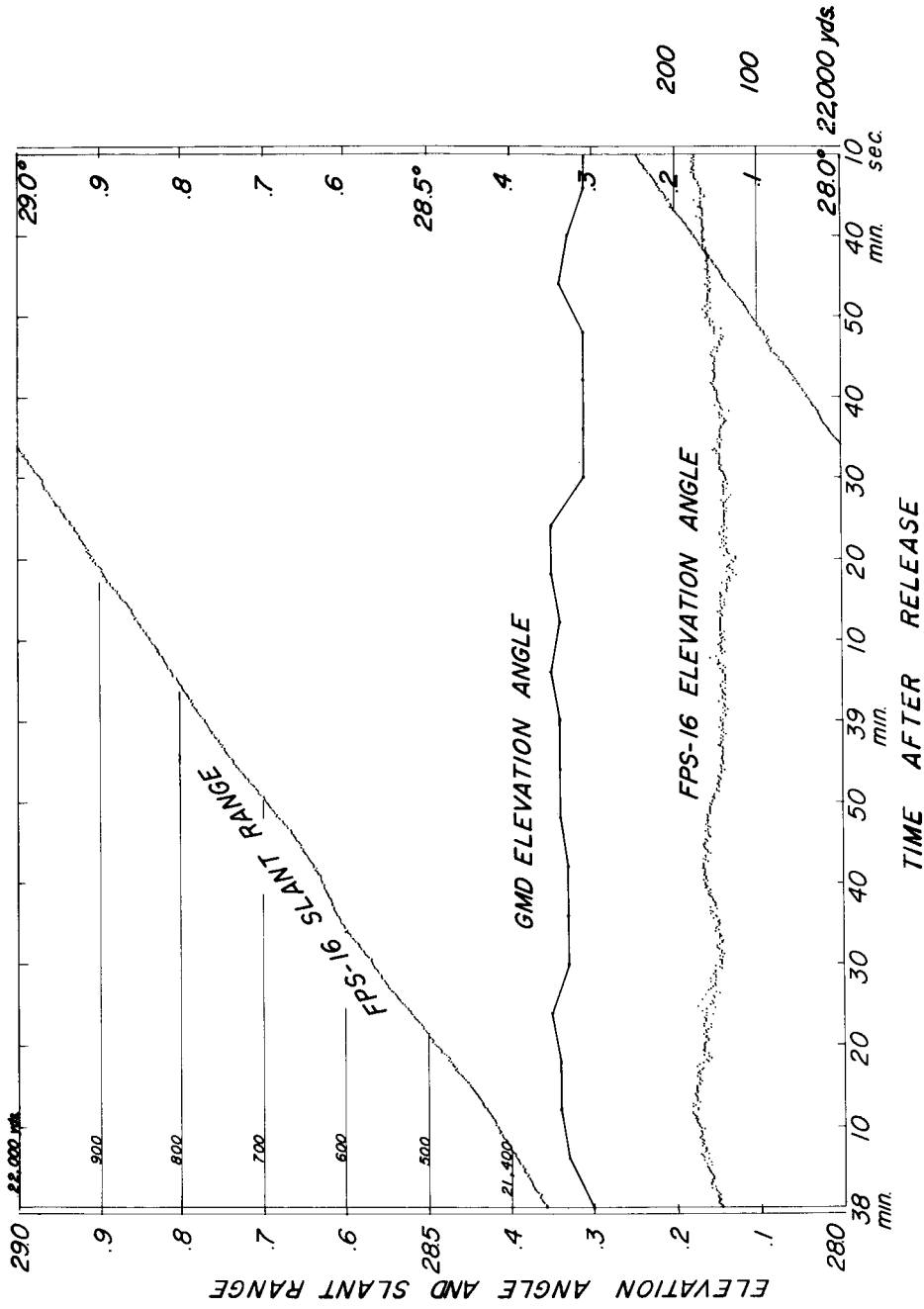


Figure 6: Comparison of GMD and FPS-16 elevation angles 38 min to 40 min 10 sec after release, February 7, 1964

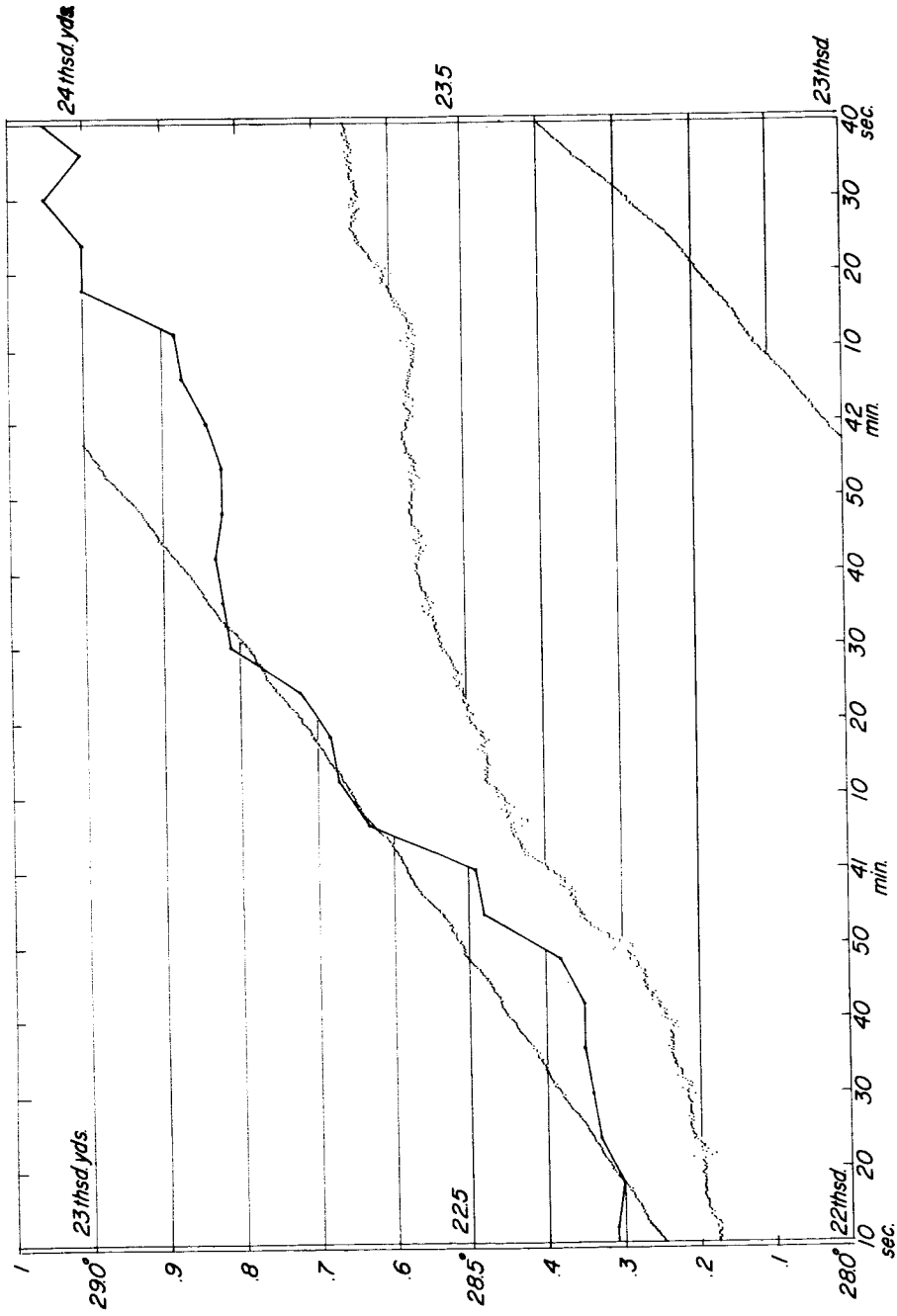


Figure 7: Comparison of GMD and FPS-16 elevation angles 40 min 10 sec to 42 min 40 sec after release, February 7, 1964

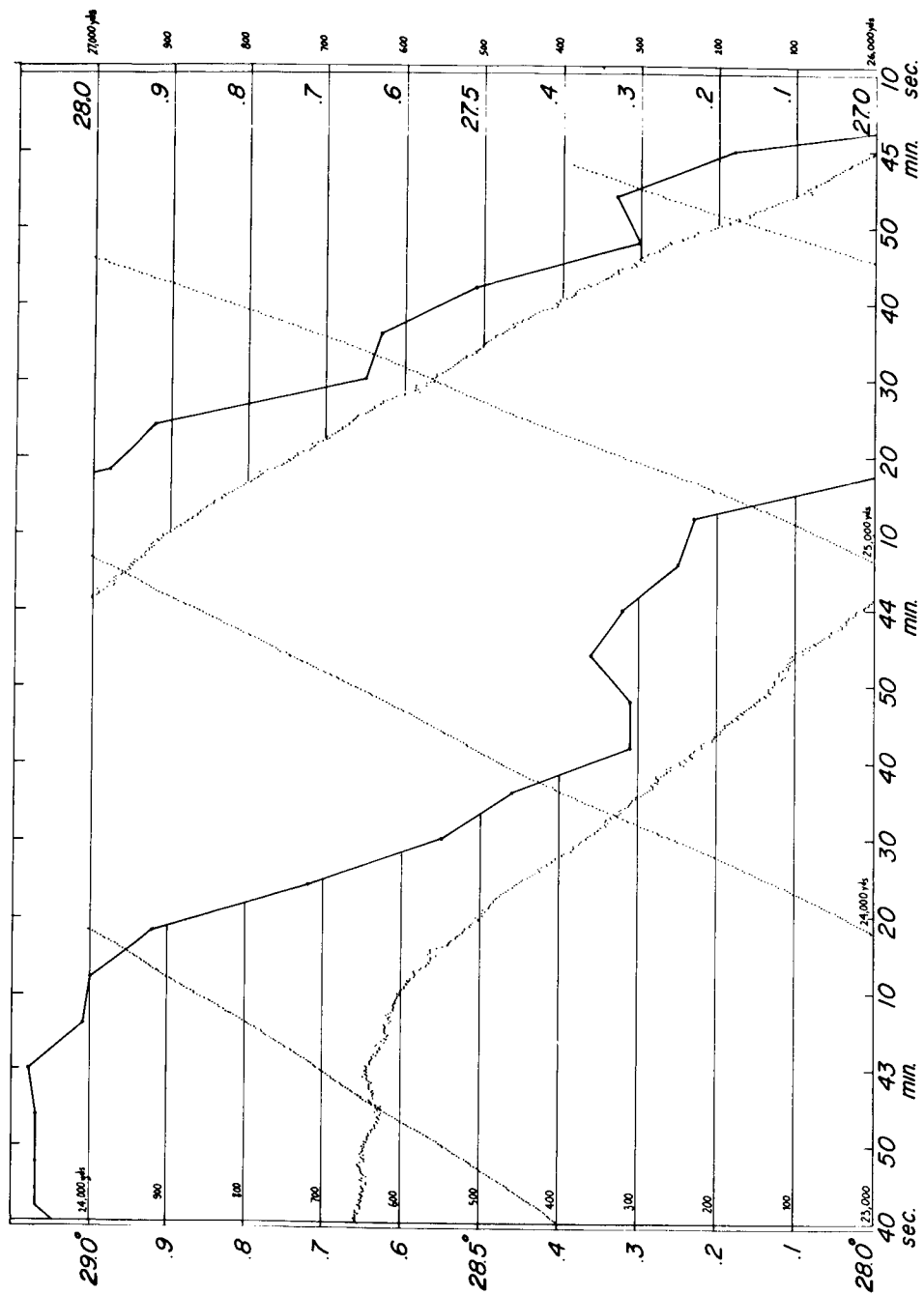


Figure 8: Comparison of GMD and FPS-16 elevation angles 42 min 10 sec to 45 min 10 sec after release, February 7, 1964

to permit identification of each value. All GMD angles, one every 6 sec, are plotted and connected by straight lines. The slant range measured by the FPS-16 are also shown in these figures. The scales on the ordinate apply directly to the FPS-16 measurements. To obtain the proper elevation angle for the GMD, 2 deg must be added to the elevation angle scale. At the initial point of Figure 6, 38 min after release, the GMD measured an elevation angle 2.15 deg greater than that measured by the FPS-16. This difference is due to parallax; the GMD was 3,363 yards east-southeast of the FPS-16 and the balloon, moving eastward, was southeast of both.

Between the 38th and 40th min, the mean elevation angle recorded by both systems was approximately constant. The deviations from the mean, however, were not well correlated. For example, the oscillation in the GMD elevation angle curve between 39 min 25 sec and 55 sec does not appear in the FPS-16 measurements. Since this totally spurious oscillation should be eliminated, averaging over more than 30 sec appears to be necessary. As the elevation angles increase, Figure 7, the trends in the two curves remained similar but once again deviations from the mean were not well correlated. The spurious oscillations in the GMD curve again had periods in the order of 30 sec.

The increasing elevation angles in Figure 7 correspond to the increased ascent rate of the balloon, discussed in Section 3C, not to a slower horizontal wind speed. This can be deduced from the approximately linear trend in the range measurements. After 42 min 20 sec, the slope of the range curve increased as the balloon entered the region of strong wind shears below the jet. With the increasing wind speeds, the elevation angles began to drop and then decreased rapidly after the 43rd min (Figure 8). Both instruments recorded the decreasing angles but the large spurious oscillations in the GMD measurements reversed the trend at 43 min 50 sec and again at 44 min 50 sec. The deviations from the mean appear to be  $\pm 0.2$  deg or 4 times the RMS error. To eliminate or strongly suppress these oscillations, at least 6 consecutive points must be averaged. This places a lower limit on the number of points or on the time interval required for averaging the GMD data.

## SECTION 5. GMD-1 DATA PROCESSING

### 5A. GMD-1 Measurements and Data Reduction

A complete set of measurements in the GMD-1 system includes pressure, temperature, relative humidity, azimuth angle, elevation

angle, and time. The azimuth and elevation angles are printed on a tape every tenth of a minute. Included in the printout are the angles in degrees and a portion of the vernier scale which can be read to the hundredths of a degree. To synchronize the tracking and thermodynamic data, the latter can be determined at the same times as the former, or the thermodynamic data can be read independently if the time of each reading is determined. The second method is preferred because the pressure is calibrated only when the baroswitch is activated at the completion of each temperature contact. For maximum accuracy, the baroswitching should also activate a timer. A timer is not included in the GMD equipment, therefore, it was necessary to assume that the time between contacts was determined by the corresponding distances on the radiosonde recorder chart. This assumption is valid if the line voltage is constant, for then the recorder chart feeds out at a constant rate.

All the necessary charts for the Pt. Mugu GMD soundings were available. Pressures were read to the nearest millibar from the calibration charts. Frequencies corresponding to temperature and relative humidity were read to the nearest tenth of an interval from the recorder charts; this provides temperature measurements accurate to the nearest one or two tenths of a degree. Times were read to the hundredth of a minute.

In the course of this study it was found that the pressure calibration chart could not be accepted literally. Friction in the baroswitch apparently produces errors in the pressure calibration. The sandwich of conductors and insulators in the baroswitch does not have a smooth surface. If the needle point on the baroswitch arm (activated by the pressure-sensing aneroid) encounters a surface irregularity, it might be held until a pressure difference develops to overcome the friction. The pressure difference would, of course, represent an error. Apparently, this friction-induced error is less probable when the instrument is swinging and bouncing in flight because of errors in ascent rate, which will be discussed later, were removed by smoothing the pressure differences between successive contacts. This implies a more uniform pressure increment between pressure contacts when the balloon was in flight than when the balloon was in the calibration chamber. The smoothing also removed roundoff errors in reading the pressure calibration chart at low pressures. When the pressure increment between contacts is less than one millibar, the reading error is of the same magnitude as the pressure increment itself. It was also found necessary to smooth the series of contact times. Errors in the timing were probably caused by non-uniform line voltages. All smoothing was done objectively as part of the computer program to be discussed next.

## 5B. Computational Methods

In the GMD-1 rawin system the pressure contacts provide the most natural interval for processing the data. By choosing the pressure contact interval as the basic interval, the thermodynamic data is specified with no interpolations. However, the time interval between contacts is not a constant; it increases as the pressure decreases. It is about 1/2 minute near the earth's surface and increases to approximately 1 minute at 100 millibars and 1 1/2 minutes at 50 millibars. If the pressure contact interval is used for computing winds as well as for specifying thermodynamic quantities, the number of observations of azimuth and elevation angle that enter each wind calculation will vary. The number varies from 5 or 6 observations per interval near the surface of the earth to about 10 or 15 at 50 mbs. Since the errors in the computed heights and in the observed elevation angles also tend to increase as the pressure decreases, averaging between the pressure contacts automatically tends to compensate for the degeneration of the data. The number of values that enters the average near the ground is also consistent with the minimum required to remove spurious oscillations as discussed in the previous section.

An arbitrary decision was made to obtain winds at the mid-point of the interval between successive contacts (to be referred to simply as "mid-points"). All measurements of azimuth angle and elevation angle between successive contacts were averaged and the mean value was assigned to the mid-point. The time and the height of the mid-point were taken to be the arithmetic means of the times and heights at the bracketing contacts. The distance out over a curved earth was computed from the mid-point height and the average elevation angle. Then the distance out and the average azimuth angle were used to compute horizontal winds by finite centered differences.

The computer program to process the GMD radiosonde data involves the following steps:

1. Editing the data to remove gross errors due to transcription or keypunching mistakes;
2. Filtering the data to remove random noise;
3. Computing the winds and their shears;
4. Checking the shears on the basis of physical credibility.

At the conclusion of the fourth step, the program either terminates by printing out the resultant information or recycles to step 2 where a more powerful filtering device is applied to the data.

Thermodynamic quantities are processed first. To remove irregularities in the GMD chart feed speed, the recorded time of each contact is smoothed by two applications of a three point average in which all points are weighted equally. To remove calibration errors and roundoff errors, the same three point average is applied 6 successive times to the pressure data. No smoothing is applied to the temperature or humidity data.

The height of each contact above the earth's surface is computed by a setwise application of the integrated hydrostatic equation between the smoothed pressure limits of successive contacts. In the integration, virtual temperature is assumed to vary as  $p^k$  between contacts. The heights are stored then the distances out and average azimuth angles are computed and stored for the wind computations.

At each mid-point the ascent rate of the balloon and the horizontal wind vector (direction and speed) is computed by finite differencing between the position coordinates at the adjacent mid-points. These two contact interval averages correspond to about a 1 min average near the surface and a 3 min average at 50 mb.

The magnitude of the curvature of the hodograph is also computed at each mid-point by the following equation

$$[ (u_1 + u_3 - 2u_2)^2 + (v_1 + v_3 - 2v_2)^2 ]^{1/2}$$

where  $u$  and  $v$  are the two wind components and the subscripts 1,2, 3 refer to successive mid-points. The winds are accepted when the magnitude of the curvature is less than 4 m/sec. In the stratosphere this is approximately equivalent to a 2 meter per second perturbation with a wavelength of 1 kilometer. The basis of this criterion will be presented later in Section 10. The curvature at the jet core can exceed 4 m/sec but this would be an isolated point, therefore all isolated points at which the criterion was exceeded were accepted. Only when the criterion was violated at several points within a limited range, was it deemed necessary to recompute the winds.

The winds were recomputed using mid-point values obtained by averaging over three contact intervals rather than one. The finite difference operations were carried out between values at mid-points four contacts apart. Wind speeds and directions were still computed at each mid-point however. The magnitude of the

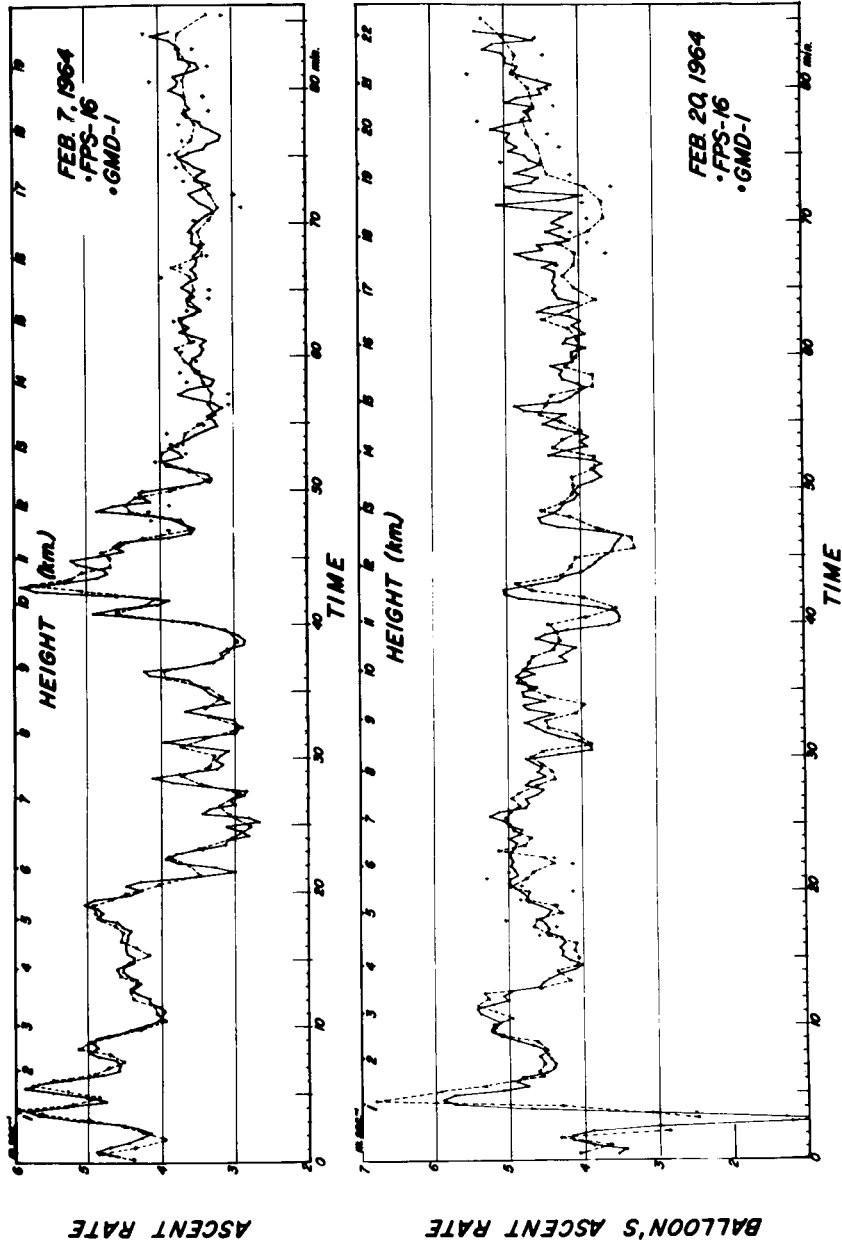


Figure 9: Balloon's ascent rates, February 7 and February 20, 1964



curvature of the hodograph was also re-computed at each mid-point and compared to the same criterion. In those cases where the criterion was not satisfied by winds based on averages over three contact intervals, an average over 5 or 7 contact intervals resulted in a hodograph that satisfied the criterion; but the hodograph contained large velocity errors spread over many successive points. Instead of increasing the averaging beyond a three contact interval, curve fitting was used to obtain the mean wind speed and direction appropriate to synoptic scale analyses. The method is discussed in Section 8.

## SECTION 6. COMPARISON OF FPS-16 AND GMD-1 ASCENT RATES AND WINDS

### 6A. Ascent rates

When ascent rates calculated from FPS-16 data are compared with those calculated from GMD-1 data, two completely different sets of measurements are involved. The FPS-16 rates were computed from thermodynamic data which are independent of the tracking data. The time intervals are also independent since the FPS-16 measurements were made at 0.1 second time intervals whereas the GMD data were obtained at a variable time interval dependent upon the baroswitch contacts.

If the ascent rates do not agree, two sources of error which contribute to errors in the GMD-1 winds must be considered:

1. An error in the mean temperature or in the limiting pressures used in the integration of the hydrostatic equation.
2. An error in the time due to an uneven feedout rate of the recorder chart. This error can be distinguished from the previous one since a significant change of feedout rate will tend to introduce a phase lag between the FPS-16 and the GMD-1 ascent rates when the ascent rates are plotted as a function of time.

Two examples of ascent rates as a function of time and height are illustrated in Figure 9. The upper graph was taken from the run of February 7, 1964; the lower graph from February 20. In both diagrams the continuous lines represent the FPS-16 ascent rates; the dash line represents the GMD ascent rates. The latter were based on the smoothed pressures. The isolated crosses represent the ascent rates computed from the GMD data using the original pressure calibration values.

In the ascent of February 7, the GMD ascent rates closely approximate the FPS-16 ascent rates from time 0 to 55 min after release. The correspondence is excellent with respect to both amplitude and phase of the departures from the mean. Because the ascent rates vary from 2.7 to 6 m/sec the height scale at the top of the diagram is non-linear. At heights greater than 13 km, the correspondence between the two rates deteriorates. Nevertheless, the correspondence between the GMD ascent rates computed from the smooth pressure data are significantly better than those based on the original calibration chart.

The curves for February 20 contain several intervals with noticeable phase differences which are attributed to variations in the feedout rate of the recorder chart. All times involved were rechecked to determine if the data had been transcribed and punched correctly; no errors were detected. Between the 17th and 25th min the crosses scattered above and below the FPS-16 curve represent errors in the pressure calibration chart probably due to friction in the baroswitching device.

Both diagrams dramatically illustrate why it is dangerous to assume a constant ascent rate for a radiosonde balloon. It is standard practice to assume a constant rate between the pressure reference contact, i.e., between every 5 contacts. This corresponds to 5 consecutive points on the dashed GMD-1 line. In 5 points, the ascent rate frequently varied from 4 to 6 m/sec or about 150%. An extreme case occurred between the third and fifth minute on the 20th of February where the rates varied 600%. Errors in winds caused by the assumption of a uniform ascent rate have been discussed by Danielsen (1959).

#### 6B. Wind Profiles and Hodographs

The winds derived from three separate balloon ascents will now be examined to determine the accuracy of the GMD computations. For each ascent, both the wind speeds profiles and the vector hodograph will be presented. In the profiles the wind speeds, in meters per second, are plotted against height, in kilometers. The FPS-16 wind speeds, computed at a constant time interval of 20 sec, are connected by straight line segments. Each speed represents a 40 sec average. The GMD wind speeds, computed at the mid-point of each pressure contact, are represented by crosses. They were not connected because most of the crosses fell on, or adjacent to the FPS-16 profiles. The temperature trace as a function of height was also plotted and can be recognized as a heavy continuous line sloping upward to the left.

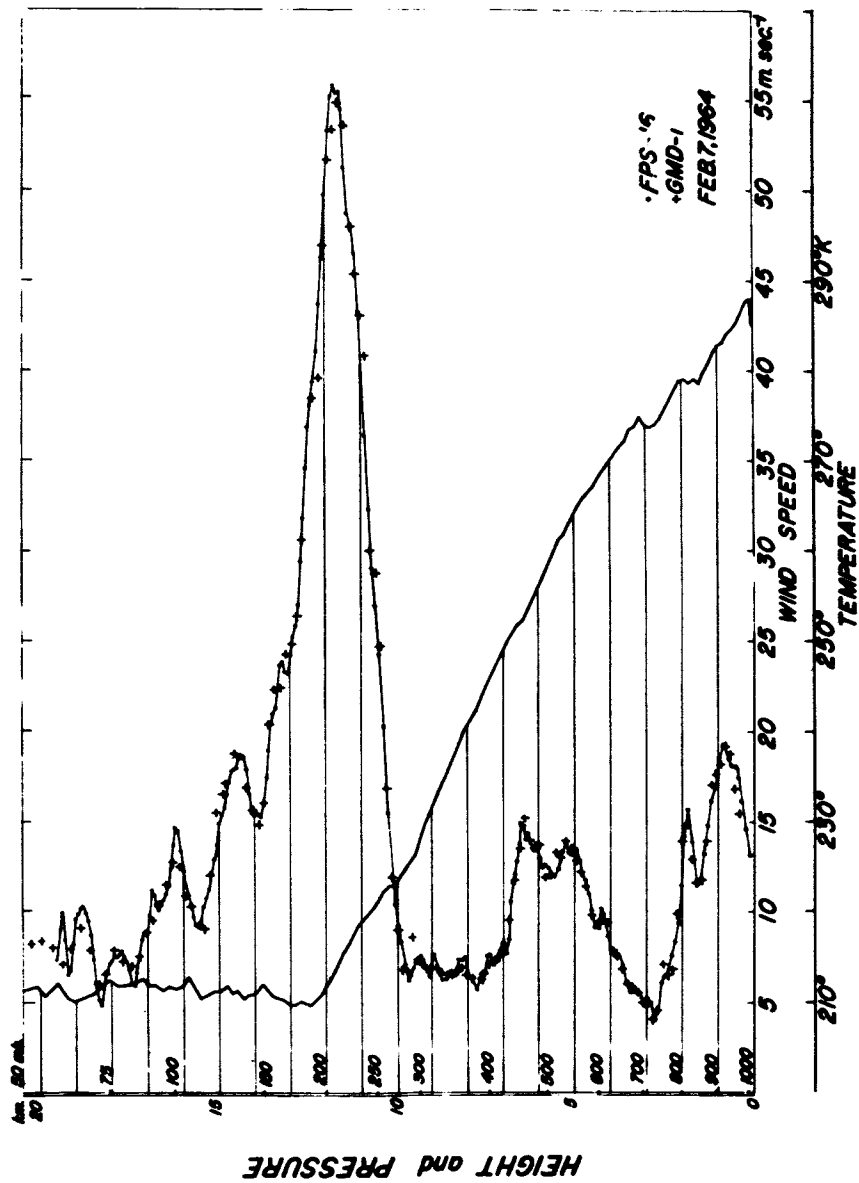


Figure 10: Wind speed and temperature profiles, February 7, 1964

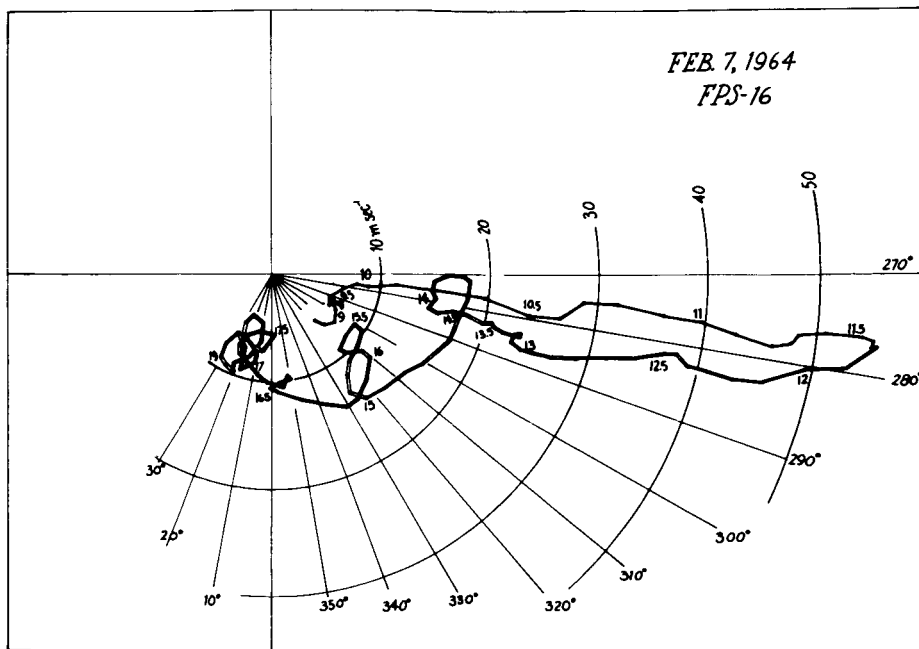


Figure 11: FPS-16 wind velocity hodograph, February 7, 1964

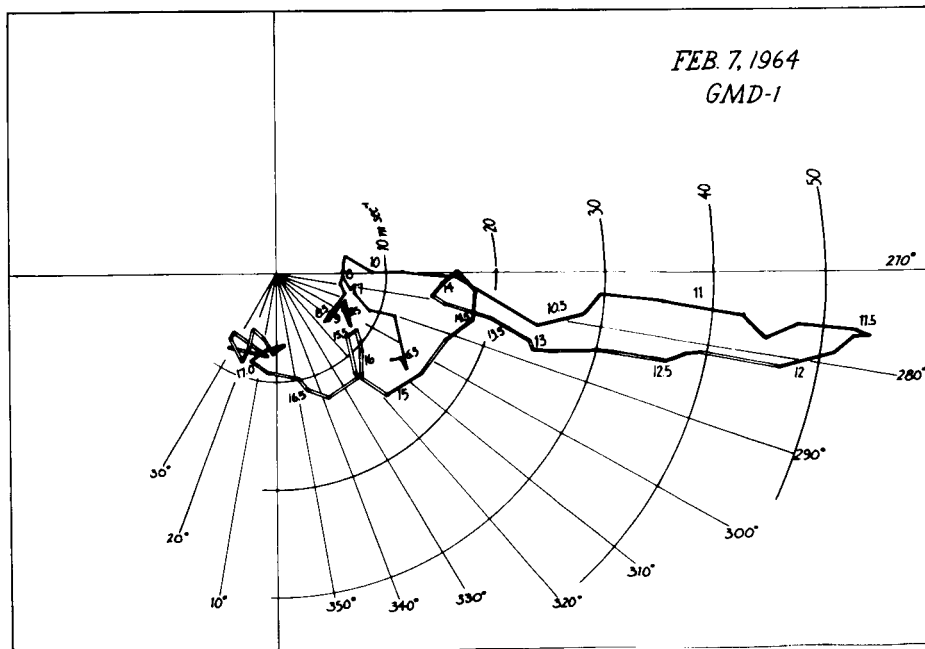


Figure 12: GMD-1 hodograph, February 7, 1964

The ordinate also contains a standard pressure scale. An appropriate temperature expressed in degrees Kelvin is the lower scale along the abscissa.

6B. (1). Ascent of February 7, 1964

Wind speeds derived from the first ascent, February 7, 1964, are presented in Figure 10. The profile is unusual because the large scale features include three maxima. The first is at an elevation of 1 km; the second, 6 km; the third, the main jet, is centered at 11.6 km. Superimposed on these macroscale features are numerous mesoscale and microscale oscillations in the wind speed. In this report, the term mesoscale will refer to wind oscillations with a vertical wave length greater than one and less than three kilometers, as for example, the oscillations between 14 and 16 km. The term microscale will apply to all shorter wave lengths such as those between the 7th and 10th km. It is clear in Figure 10 that the GMD winds reproduce both the macroscale and mesoscale features of the wind profile from the surface to 19 km. Within this interval only the microscale features were distorted or eliminated. Since the two profiles were computed from completely independent sets of measurements there can be little doubt about the existence of both the macroscale and mesoscale features.

Oscillations in wind direction can be seen in the hodograph plotted from the FPS-16 wind vectors, Figure 11, and the GMD-1 wind vectors, Figure 12. The complete hodographs were complicated by many overlapping points. Therefore, the wind vectors in the lowest 8 km were eliminated from Figure 11 and those in the lowest 6 km were eliminated in Figure 12. To aid the reader in tracing the hodograph as a function of height, the heights in kilometers have been plotted adjacent to the appropriate points. Also, the observations up to the jet core have been connected with a heavy black line while those above the jet core were connected by a double line. When the hodograph closes on itself or loops, it has been drawn to give the impression of a rope folded over itself. With this optical device it is possible to decipher some extremely convoluted patterns.

A comparison of Figures 10 and 11 shows that oscillations in the wind speed correlate with oscillations in wind directions, i.e., the oscillations of 10.5 and 11.2 kilometers correspond to undulations in the hodograph. The mesoscale speed oscillations at 14 and 16 kilometers also correspond to loops in the hodograph. Note, in particular, that the loop at 14 kilometers was produced

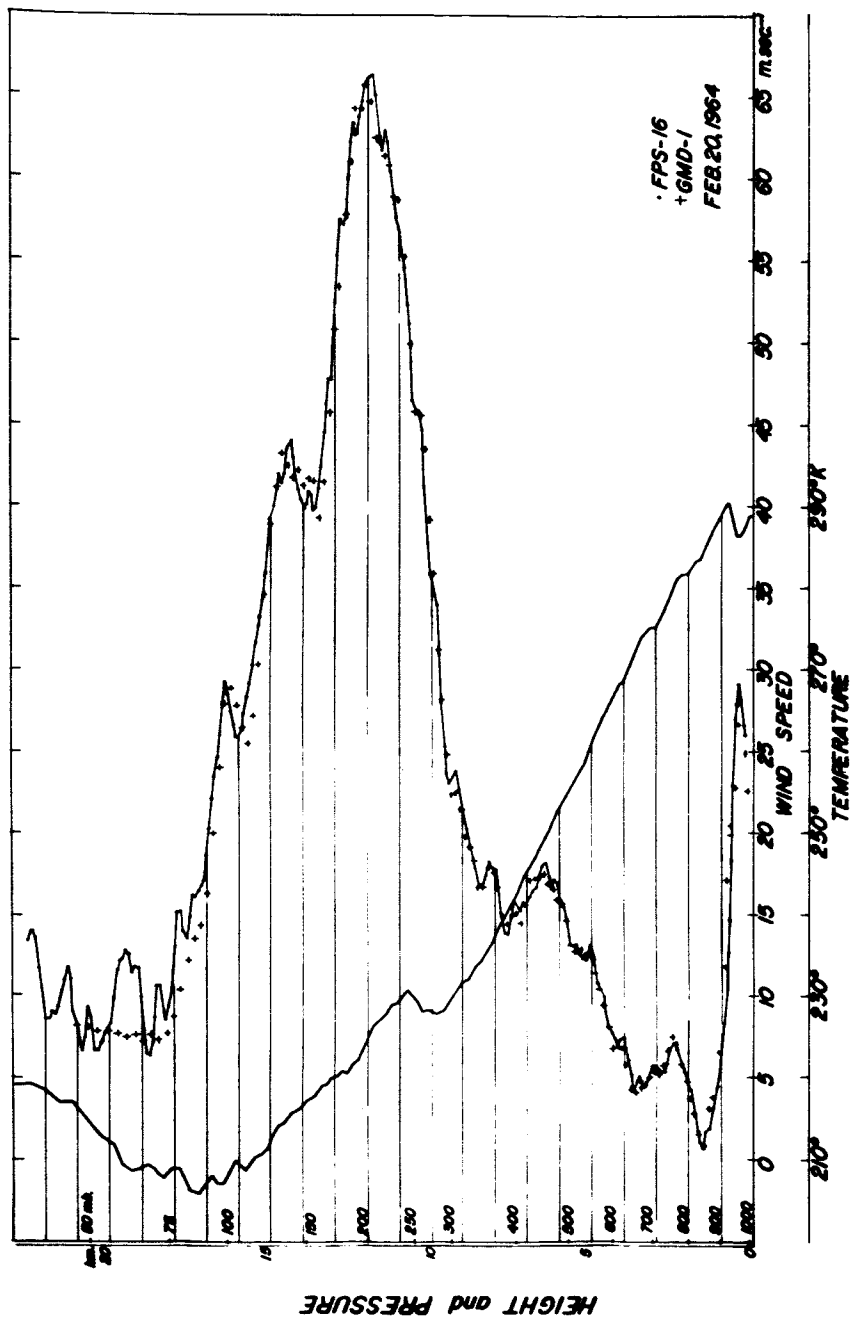


Figure 13: Wind speed and temperature profiles, February 20, 1964

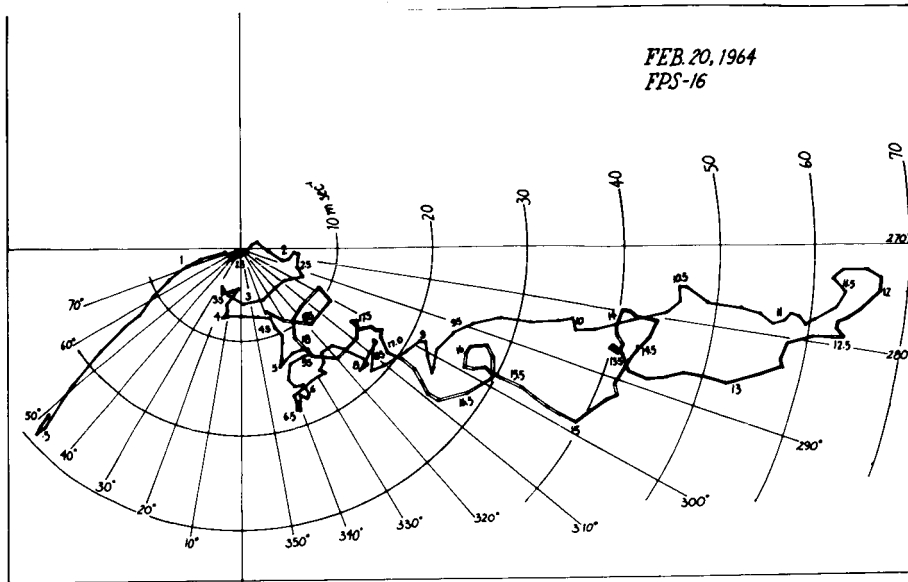


Figure 14: FPS-16 wind velocity hodograph, February 20, 1964

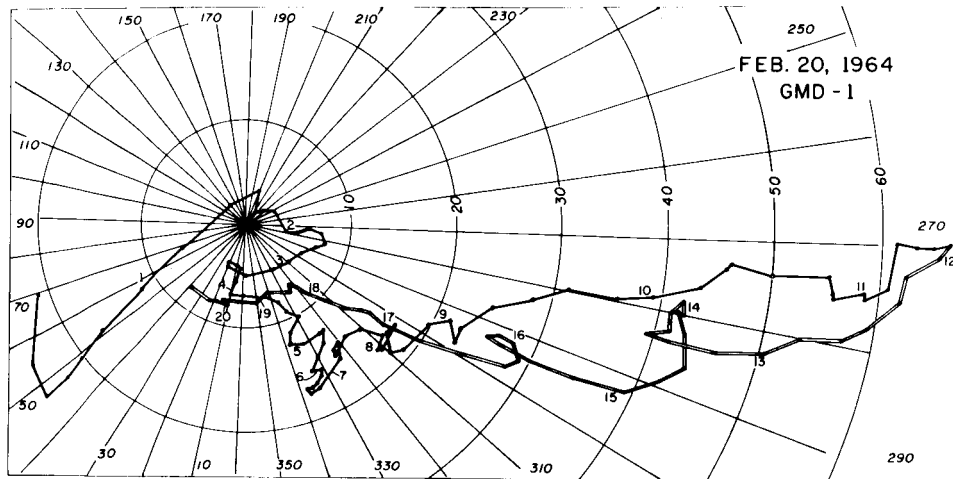


Figure 15: GMD-1 hodograph, February 20, 1964

by an anticyclonic turning of the wind vector with height.

The remarkably close correspondence between the GMD-1 and the FPS-16 wind speeds and wind vectors indicates the potential of the GMD-rawin system. With few exceptions, the wind speeds are accurate to within  $\pm 1$  m/sec and the wind directions to within  $\pm 2$  deg. The maximum error in speed at an isolated point is 2 m/sec and the maximum error in wind direction is  $\pm 5$  deg.

#### 6B. (2). Ascent of February 20, 1964

The wind speed profile for February 20 (Figure 13) contains two maxima. The first maximum of 28 m/sec at 0.05 km presents the downslope Santa Anna Wind. In the next kilometer, the speeds decrease rapidly to almost zero. Above this level the wind speeds increase to a strong jet of 67 m/sec at 12 km then decrease to a minimum of 10 m/sec at approximately 19 km. Once again, numerous mesoscale and microscale oscillations are superimposed on the mean profile. From the surface to 13 km, the GMD wind speeds correspond closely to the FPS-16 wind speed profile but above this level, errors of 3 and 4 m/sec are evident. These errors distort the mesoscale oscillation at 14 km and displace the minimum at 16 km to a slightly lower level. Above the 17 km level, the increasing number of data points which enter the averages in the GMD-1 calculations completely smooth out the mesoscale oscillations. One notices, however, that the mean GMD speeds are consistently lower than the mean of the FPS-16 measurement. If the reader refers back to Figure 9, he will notice that the ascent rate calculated from the GMD data was slower than that of the FPS-16 between the 17 and 20 km. The corresponding errors in ascent rate and speed are probably caused by a faster than normal feedout rate of the recorder chart. The chart intervals between successive contacts is then overestimated and the speed underestimated. However, some of the errors can be attributed to errors in measurements in elevation angles for the accuracy of the elevation angle measurements degenerates as the elevation angles decrease. Since the mean wind speed on February 20 was greater than that of February 7, generally lower elevation angles were encountered.

The hodograph (Figure 14) plotted from the FPS-16 winds of February 20th is complicated by numerous reversals, undulations and loops. However, the hodograph (Figure 15) plotted from the GMD-1 winds reproduces all the zigs and zags in the FPS-16 hodograph but the correspondence is not always exact. The



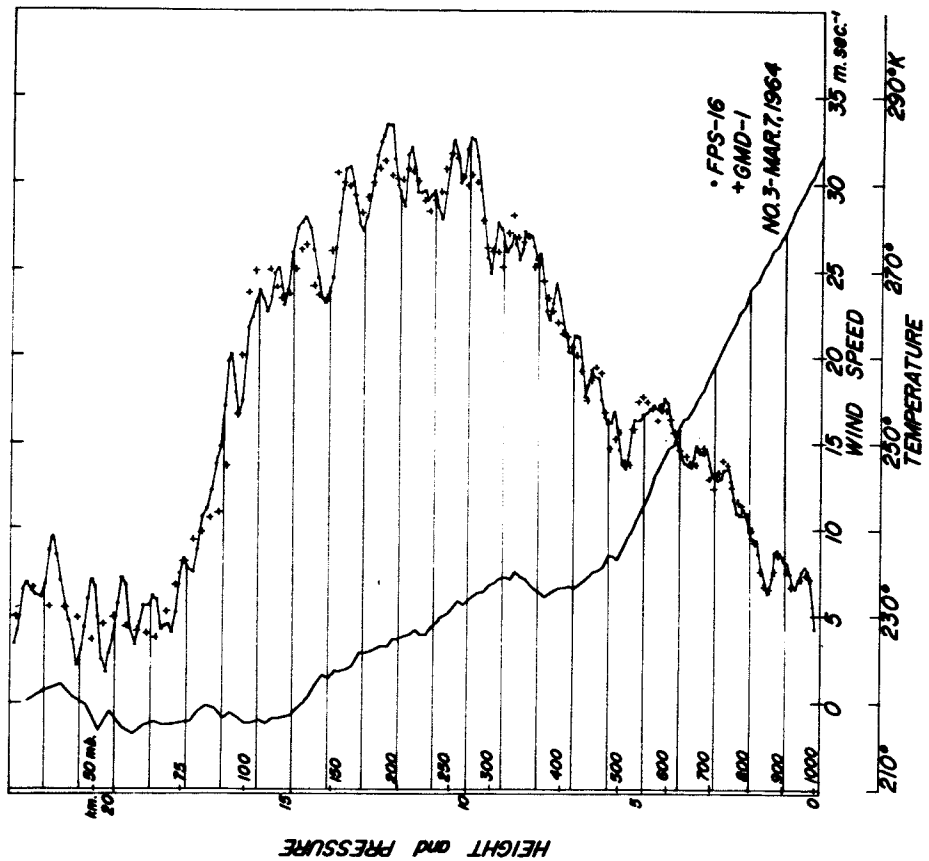


Figure 16: Wind speed and temperature profile for 3rd ascent of March 7, 1964, (1659Z)

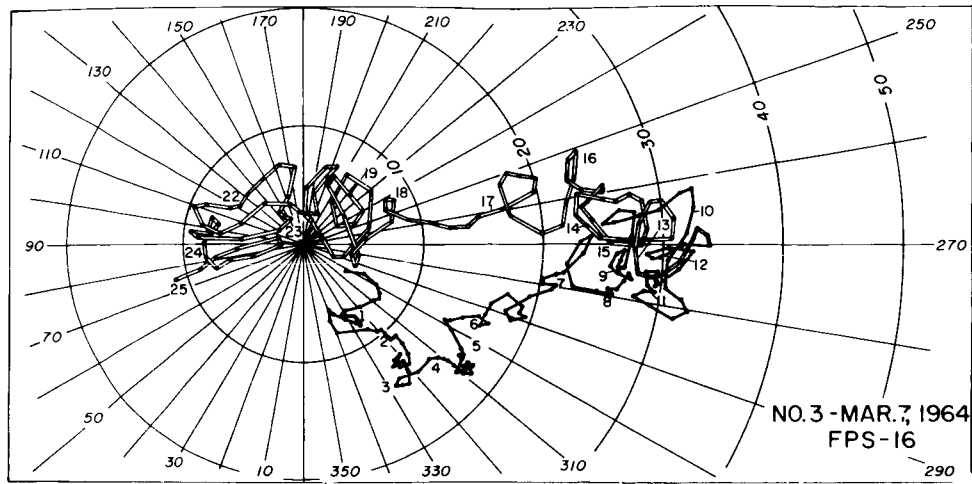


Figure 17: FPS-16 hodograph for 3rd ascent of March 7, 1964

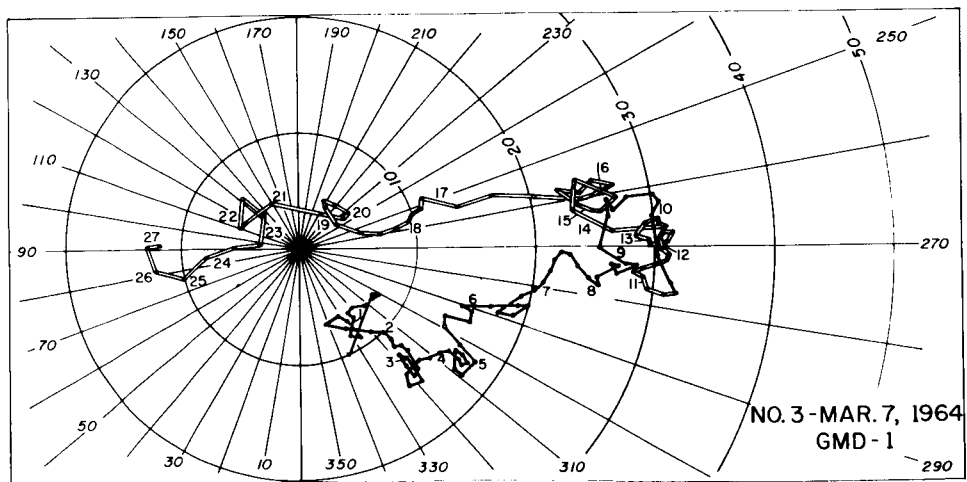


Figure 18: GMD-1 hodograph for 3rd ascent of March 7, 1964

anticyclonic loop at the 14 km level is distorted but it is still an identifiable feature. Above the 17 km level the increased smoothing eliminates the loops but traces of the loop at 18.5 km appear in the form of a reduced shear. Notice that in the FPS-16 hodograph the loops at 14, 16 and 18.5 km all correspond to anticyclonic rotations.

#### 6B (3). Third Ascent of March 7, 1964

Three ascents made on March 7, 1964 were used in this study. The two earliest ascents presented a special problem and discussion of these will be postponed until the next section. •

The FPS-16 profile, (Figure 16), of the third ascent of March 7 (1659Z) contains many mesoscale and microscale oscillations superimposed on a blunt low speed jet centered at approximately 12 km. The GMD wind speeds reproduce the large scale profile and many of the mesoscale features. The largest errors (approximately 3 m/sec) occur at 16 and 17 km. Once again, the oscillations above the 18 km level are virtually eliminated by the increased number of points within each contact interval.

The hodograph plotted from the FPS-16 winds, Figure 17, inspired the comment, "It looks like an explosion in a spaghetti factory". Indeed it is extremely complicated, but if care is taken it can be deciphered. Between the 3 and 7 km level there are several small anticyclonic loops in the hodograph. Between 7 and 13 km there are both anticyclonic and cyclonic loops but above the jet core the loops are predominately anticyclonic. The GMD hodograph, Figure 18, bears a close resemblance to the FPS-16 hodograph up to about the 10 km level. Above this level there is a considerable loss of detail in the mesoscale features. The loss of detail consists primarily of a suppression of the deviations from the mean and results in large directional errors at many points between 18 and 24 km. The GMD winds, however, do provide a reasonable estimate of the variations of the mean wind over this height interval.

#### 6C. Difficulties Associated with Very Low Elevation Angles

In the three examples just presented, the method developed for computing winds from the GMD data proved to be highly satisfactory. However, in all three cases, the elevation angles were never less than 10 deg. An example will now be presented which illustrates the breakdown of the method when the elevation angle was very low. At the time of the first ascent on March 7, 1964, (at 0043Z) the average wind speeds were quite high. The speed

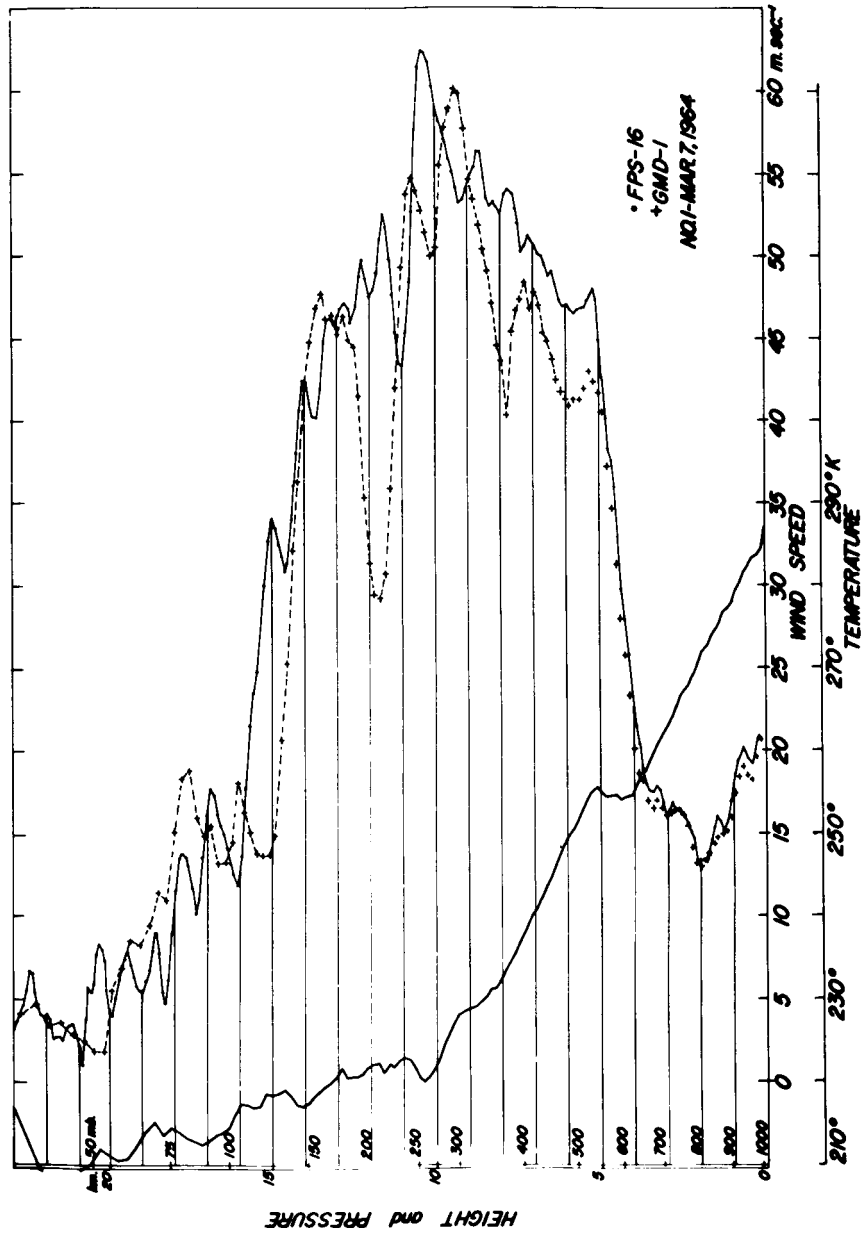


Figure 19: Wind speed and temperature profile for 1st ascent, March 7, 1964 (0043Z)

profile is plotted in Figure 19. The GMD winds agreed with the FPS-16 winds up to 3 km. Above this level the GMD winds were 4 to 6 m/sec slower than the FPS-16 winds. Above the 8 km level, errors as great as 25 m/sec were produced by the GMD data. The profile in Figure 19 represents the speeds computed from data averaged over 3 contact intervals. The initial winds contained still larger errors.

Clearly, these results are unacceptable. Increasing the averaging interval to 5 and 7 contact intervals produced no substantial improvements. The larger interval reduced the magnitude of the speed errors, but spread them over more points. It was therefore considered necessary to examine the elevation angles in detail to determine the characteristics of the errors and then to attempt other methods of smoothing which might at least preserve the mean wind speeds.

#### SECTION 7. DETERMINATION OF ERRORS IN GMD ELEVATION ANGLES

A direct comparison of the elevation angles measured by the GMD with those measured by the FPS-16 is complicated by the difference in the elevation angle produced by parallax. The effect of parallax can be removed, however, by simply transforming the FPS-16 measurements over to the position of the GMD-1 rawin system. In the transformation equations, the curvature of the earth can be neglected because this produces an error of approximately 0.02 deg, which is negligible, in comparison to the GMD errors.

The equations relating the azimuth and elevation angles which would be measured at the GMD site to the azimuth and elevation angles measured by the FPS-16 are as follows:

$$D_G^2 = D_F^2 + D_{GF}^2 - 2D_F D_{GF} \cos \Delta \alpha$$

$$\Delta \alpha = \alpha_R - \alpha_F$$

$$\epsilon_G = \tan^{-1} \left( \frac{D_{GF}}{D_G} \tan \epsilon_F \right)$$

$$\alpha_G = \alpha_F - \sin^{-1} \left( \frac{D_{GF}}{D_G} \sin \Delta \alpha \right)$$

where  $D_G$  is the horizontal distance between the balloon and the GMD

$D_F$  is the horizontal distance between the balloon and the FPS-16

$D_{GF}$  is the horizontal difference between the GMD and the FPS-16

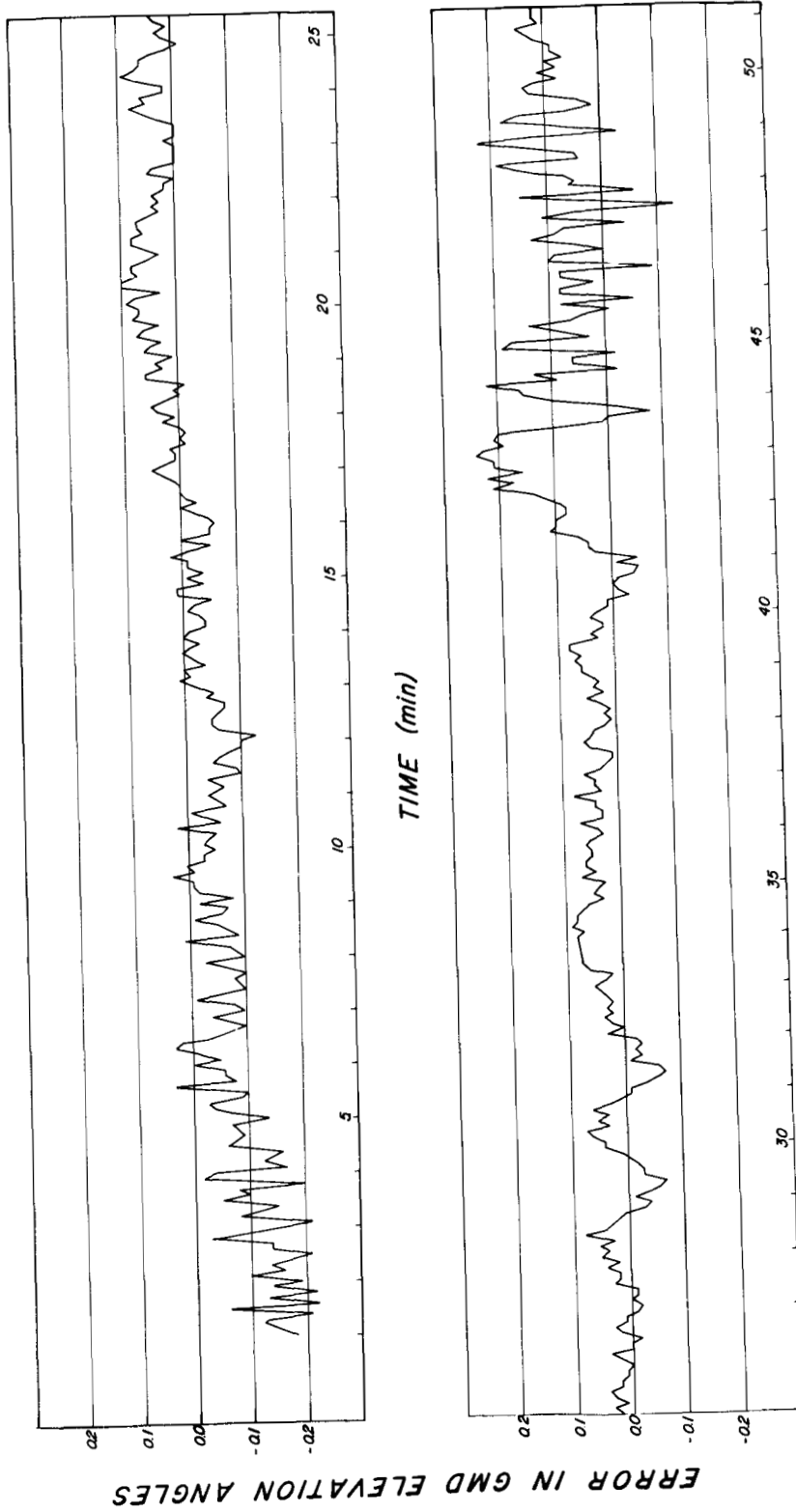


Figure 20: Errors in GMD elevation angles, February 7, 1964

$\alpha_G$  is the azimuth angle to the balloon at the GMD site

$\alpha_F$  is the azimuth angle to the balloon at the FPS-16 site

$\alpha_R$  is the azimuth angle to the GMD at the FPS-16 site

$\epsilon_G$  is the elevation angle of the balloon at the GMD site

$\epsilon_F$  is the elevation angle of the balloon at the FPS-16 site

Errors in the elevation angles measured by the GMD system during the ascent of February 7 were relatively small. As shown in Figure 20, maximum errors were slightly greater than 0.2 deg. One notices that the errors were predominately negative during the early portion of the run and predominately positive during the latter portion of the run. The change from negative to positive departures was associated with a change from large to small azimuth angles and was probably due to a small tilt in the GMD-1 radar antenna. Although the root mean square error was only slightly greater than 0.05 deg, there are certain periods when the errors were organized to form long period oscillations. Errors of this type are serious.

In Figure 21, which is taken from a portion of the ascent of February 20, both the elevation angles observed by the GMD and those adjusted for parallax are plotted so that one can compare the deviations as the elevation angle changed. The times corresponding to the lower curve are to be read from the lower abscissa and those corresponding to the upper curves from the upper abscissa. The GMD measurements are connected by a thin line; the FPS-16 measurements in this case are represented by crosses. It should be pointed out that only one out of every 60 observations made by the FPS-16 has been plotted. The dots along the GMD trace are the mean elevation angles produced by smoothing over five contact intervals. Note that the adjusted FPS-16 measurements, although scattered by  $\pm 0.03$  deg, form a very smooth mean curve. Against this smooth curve, the GMD measurements oscillate, sometimes sinusoidally and sometimes with abrupt steps of 0.1 and 0.2 deg.

Errors of the same type, but larger in magnitude, are also evident in Figure 22. These measurements were taken from the first ascent of March 7. The GMD measurements have been connected by straight line segments and are seen to oscillate about a smooth curve. The latter represents a fourth order polynomial fit to the measurements by the least squares method. The FPS-16 measurements adjusted for parallax were consistently lower than those

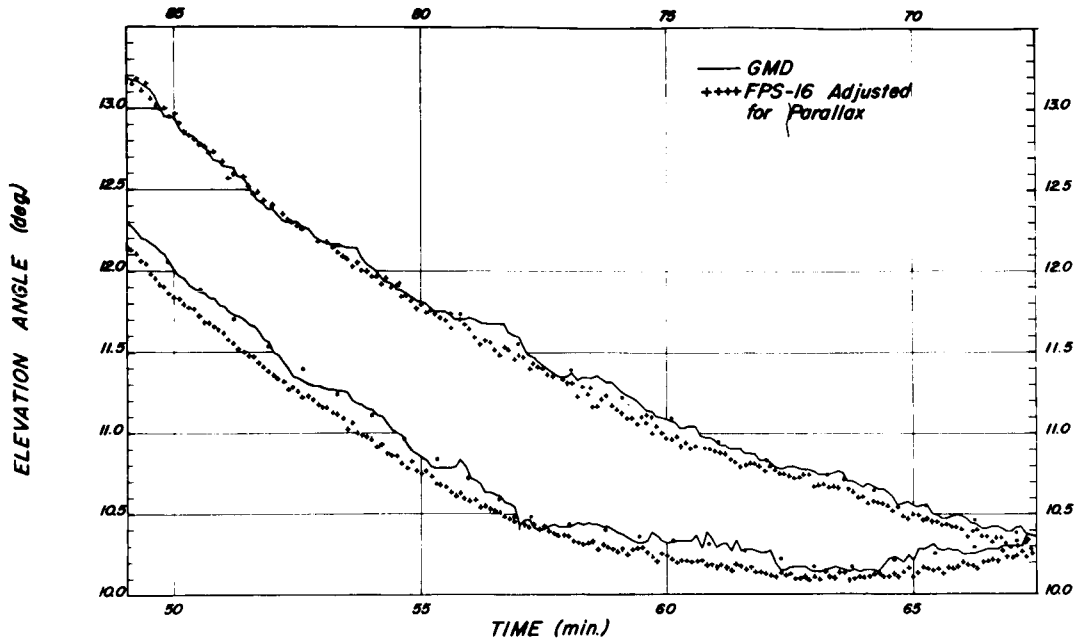


Figure 21: GMD and parallax adjusted FPS-16 elevation angles, February 20, 1964

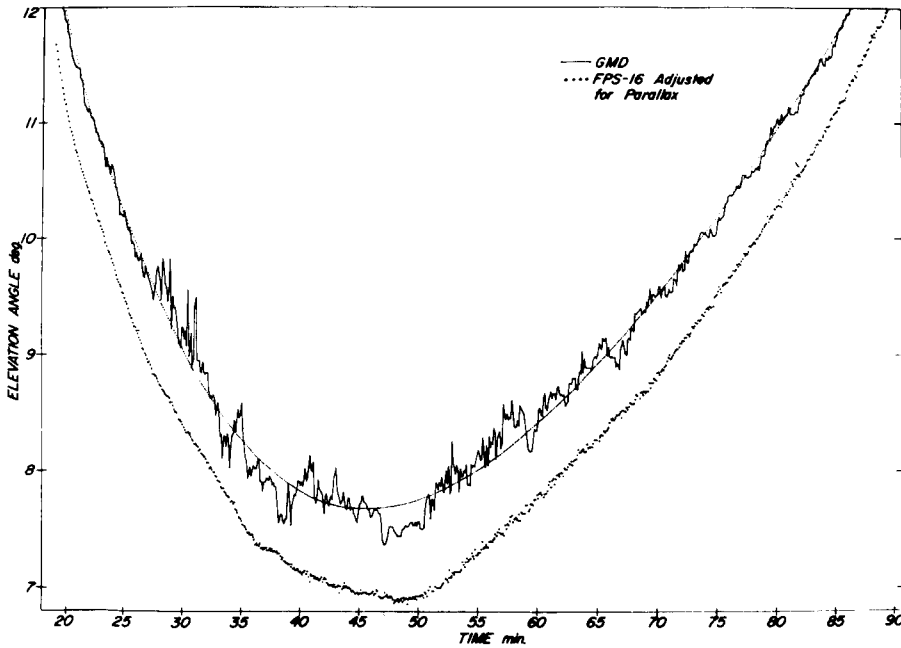


Figure 22: GMD and parallax adjusted FPS-16 elevation angles plus fourth order polynomial fit, 1st ascent of March 7, 1964, (0043Z)



measured by the GMD. An error of 0.69 deg was evident throughout the entire ascent. Since the magnitude of the error was independent of the azimuth angle, it must be due to a calibration error not to a tilt in the GMD-1 antenna. A similar error of 0.65 deg was found in the elevation angle data from the second ascent of March 7, which was made 11 1/2 hrs after the first ascent. However, at the time of the third ascent, approximately 6 hrs later, no systematic error was found. Presumably an adjustment had been made in calibration of the elevation angles between the second and third ascent.

As noted earlier in connection with Figure 21, the FPS-16 elevation angles trace out a relatively smooth curve. The scatter in the observations increases when the elevation angles are at a minimum, but the deviations in the smooth curve are usually less than 0.03 of a degree. That is, only three times the RMS error generally accepted for the FPS-16 measurements. The reader is also reminded that the FPS-16 data plotted in Figure 22 represent 1/60th of the observations; they are plotted at the same frequency as the GMD measurements.

When the elevation angles are greater than 10 deg, the GMD measurements rather closely approximate the FPS-16 measurements. At lower angles, however, the oscillations suddenly increase in magnitude. Deviations from the mean of 0.3 deg are frequent and occasionally the error increases to 0.7 deg or fourteen times the commonly accepted RMS error. One notices, also, that the deviations were predominately of the same sign for periods of the order of 5 to 7 min. The combination of large amplitude and a long period organization in the errors makes it extremely difficult to recover a properly smoothed curve by averaging over discreet intervals or by using running averages.

#### SECTION 8. GMD-1 DATA PROCESSING FOR VERY LOW ELEVATION ANGLES

The smoothness of the curve traced by the FPS-16 elevation angles in Figure 22 suggests that the large scale features of the wind could be retained if a relatively low order polynomial function were substituted for the elevation angles between the 20th and 90th min. The order of the polynomial was determined by testing the fit obtained from orthogonal polynomials. In particular, the Gram-Schmidt orthogonal polynomials were used since this set of functions is orthogonal at a discreet set of points. This feature means that, in the conventional "least squares" method of curve fitting, it is unnecessary to compute the sums of products of point values and combinations of polynomial terms. (By the definition of orthogonal functions combinatorial

terms are identically zero.) It also eliminates the need for solving a set of simultaneous equations for the coefficient of the various terms in the polynomial. The coefficient of each term can be obtained independently of the coefficients of other terms. Not only is this convenient and efficient from the computational point of view, but, in addition, it allows ready determination of the efficiency of various order polynomials. The advantages of orthogonal polynomials in curve fitting by the least squares method have been discussed in detail by Forsythe (1957).

Polynomials of order 3 through 10 were fitted to the elevation angles obtained from the first sounding of March 7. The root mean square difference between polynomial values and observed values was computed for each order polynomial. The RMS difference decreased from 0.27 deg for the third order polynomial to 0.14 deg for the fourth order and 0.11 deg for the fifth order. Higher order polynomials did not reduce the RMS difference below 0.1 deg. The dotted line passing through the GMD elevation angles in Figure 22 is the fourth order polynomial fit to those values. This confirms the subjective impression that the main features of the elevation angle distribution through a large time range can be reproduced by a relatively low order curve. Similar tests with other soundings showed essentially the same results.

The method of processing GMD-1 data (discussed in Section 5) was modified to include curve fitting when the curvature criterion is violated at more than one point after the averaging has been increased to three contact intervals. A fourth order polynomial is fitted to all elevation angles within the segment of curvature violation plus ten contact intervals at each end of the segment. The overlap is included to ensure a smooth transition in the winds computed by the two sets of data.

Curve fitting to the heights, azimuth angles and times was not considered necessary because the accuracy of these measurements did not seriously degenerate at low elevation angles. However, to ensure some modicum of consistency between the scale on which the elevation angles were determined and the scale of the other parameters, the averaging interval for the azimuth angle was extended to five contacts and the finite differencing was enlarged correspondingly. The elevation angles at each mid-contact point were also obtained from five contact interval averages of the values given by the polynomial.

To determine the amount of degradation in the GMD data that results from the use of curve fitting over long periods, the winds

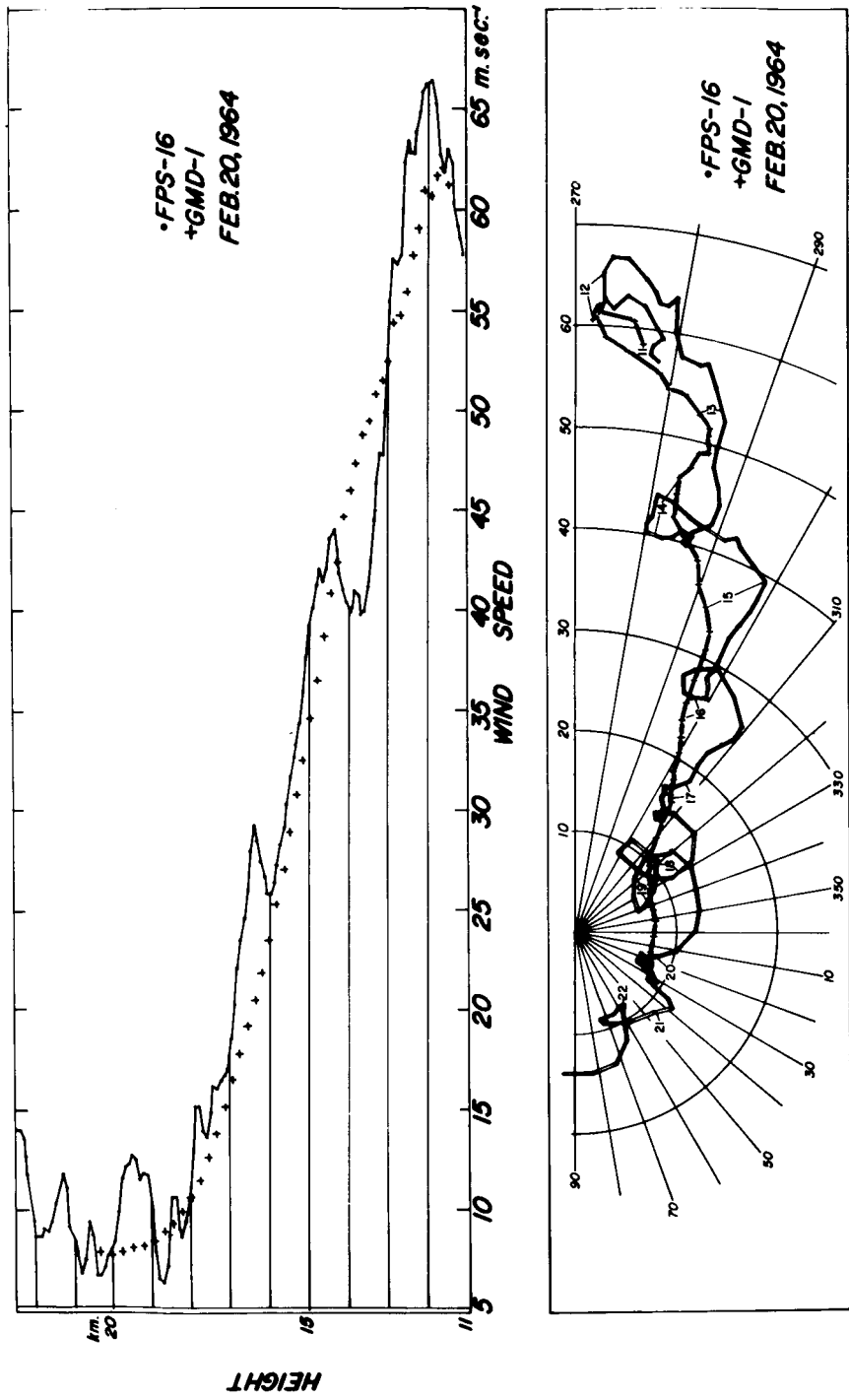


Figure 23: Winds based on polynomial fit to elevation angles, February 20, 1964

for February 20 were recomputed using a fourth order polynomial fitted to the GMD-1 elevation angles from the level of the jet maximum to the top of the sounding. The upper part of Figure 23 reproduces the top of Figure 13. It shows the vertical profile of wind speed computed from FPS-16 elevation angles as a solid line and the profile obtained from a polynomial by a series of crosses. The vector hodograph for both the FPS-16 and the polynomial winds over the same portion of the sounding is shown in the lower part of Figure 23. The FPS-16 values are joined by a double line and the polynomial values by a heavy solid line.

The wind speeds computed from the polynomial correspond closely to the mean of the FPS-16 wind speeds except the former are 3 to 5 m/sec slower than the latter between the 15th and 18th km. The mean wind direction is also well represented by the polynomial winds because the hodograph passes through the loops in hodograph of the FPS-16 winds.

#### SECTION 9. WIND COMPARISONS AT VERY LOW ELEVATION ANGLES

##### 9A. First Ascent of March 7, 1964

Winds derived from the one and three contact interval averages failed to meet the curvature criterion above 8 km in the first ascent of March 7. A fourth order polynomial was therefore fitted to all elevation angles above 6.5 km. But the elevation angles also contained a systematic error of +0.69 deg. This error was first removed and then the winds were all recomputed using a one contact interval up to 8 km and the polynomial above 6.5 km. In the 1.5 km overlap the winds were blended to provide a smooth transition.

The results are presented in Figure 24 as crosses superimposed on the same FPS-16 profile as in Figure 19. The speeds computed from the polynomial approximate the mean of the FPS-16 but the former are again 3 - 5 m/sec slow between the 13th and 15 km and too fast between the 16th and 18th km. Considering the large errors in the original GMD measurements, (Figure 22), and the large errors in the three contact averaged winds (Figure 19), the polynomial method recovers reasonably accurate mean wind speeds. In this case, a higher order polynomial might improve the accuracy, but generally, as the order is increased, a reduction in some errors is accompanied by an increase in others or the generation of new errors.

It is interesting to note that the polynomial method places the jet at 8.6 km with a speed of 58 m/sec, while the jet in the FPS-16 profile is at 10.5 km with 62 m/sec. The jet in the mean

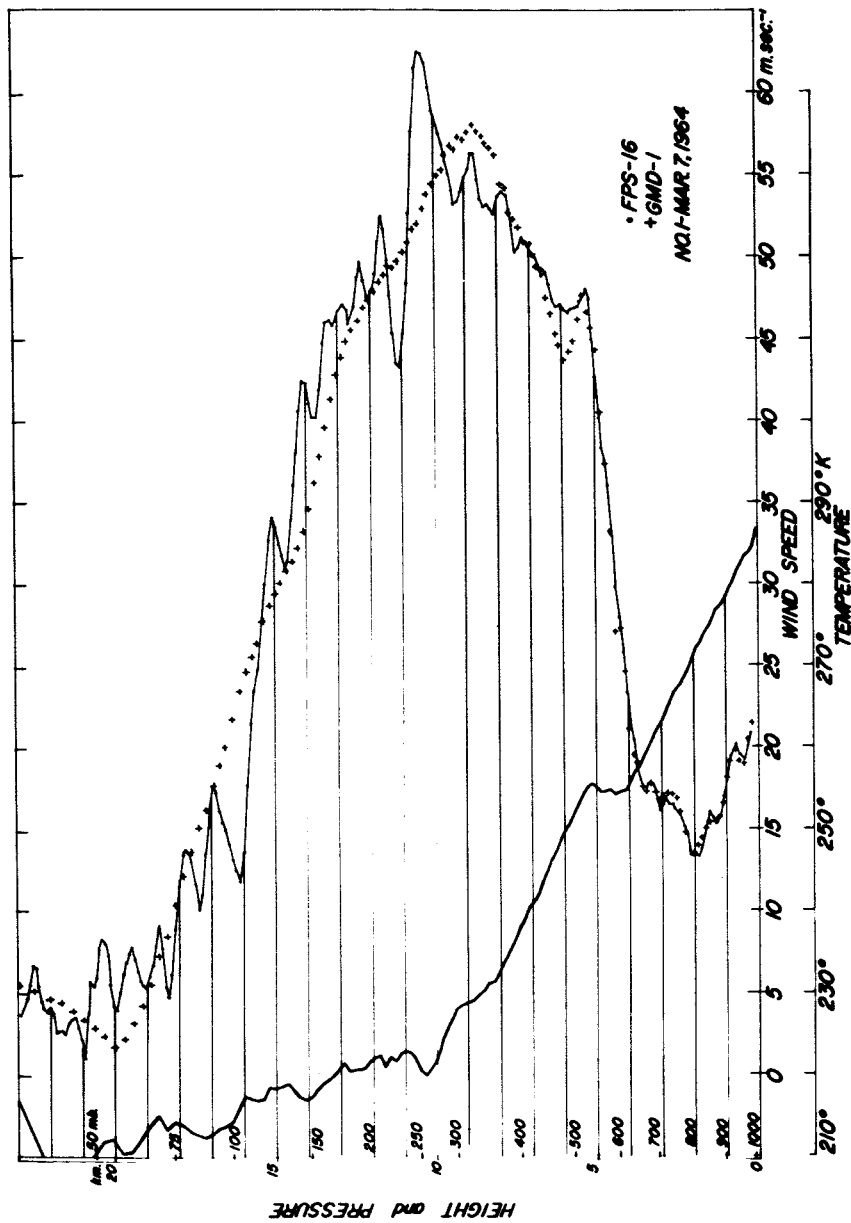


Figure 24: Wind speed and temperature profiles for 1st ascent, March 7, 1964

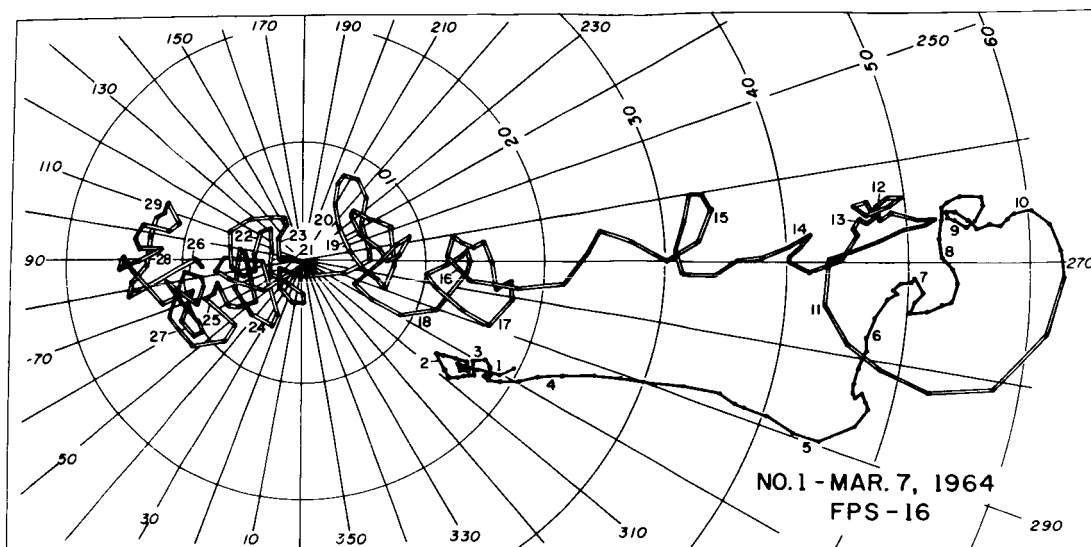


Figure 25: FPS-16 hodograph, 1st ascent, March 7, 1964

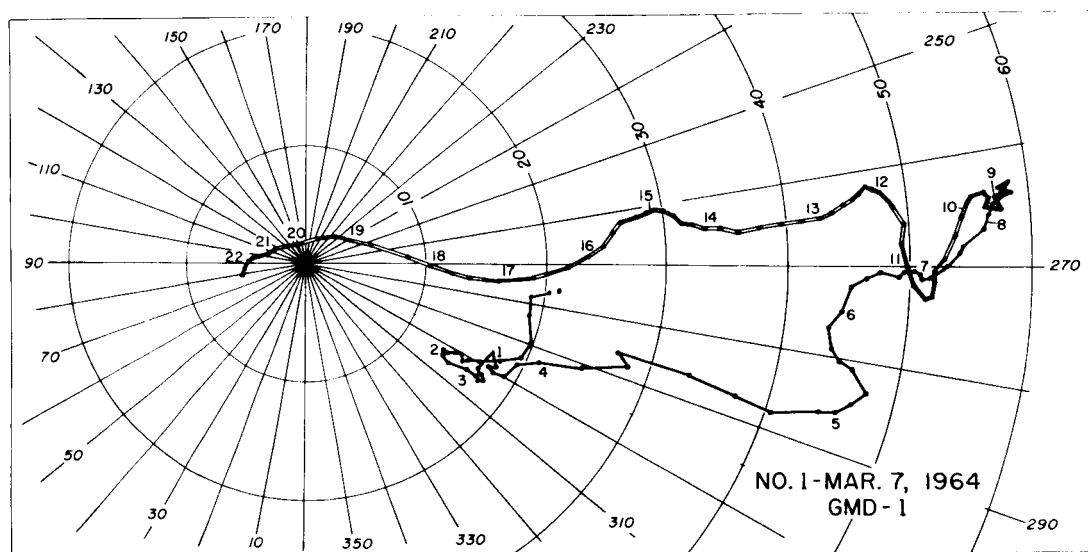


Figure 26: GMD-1 hodograph, 1st ascent, March 7, 1964

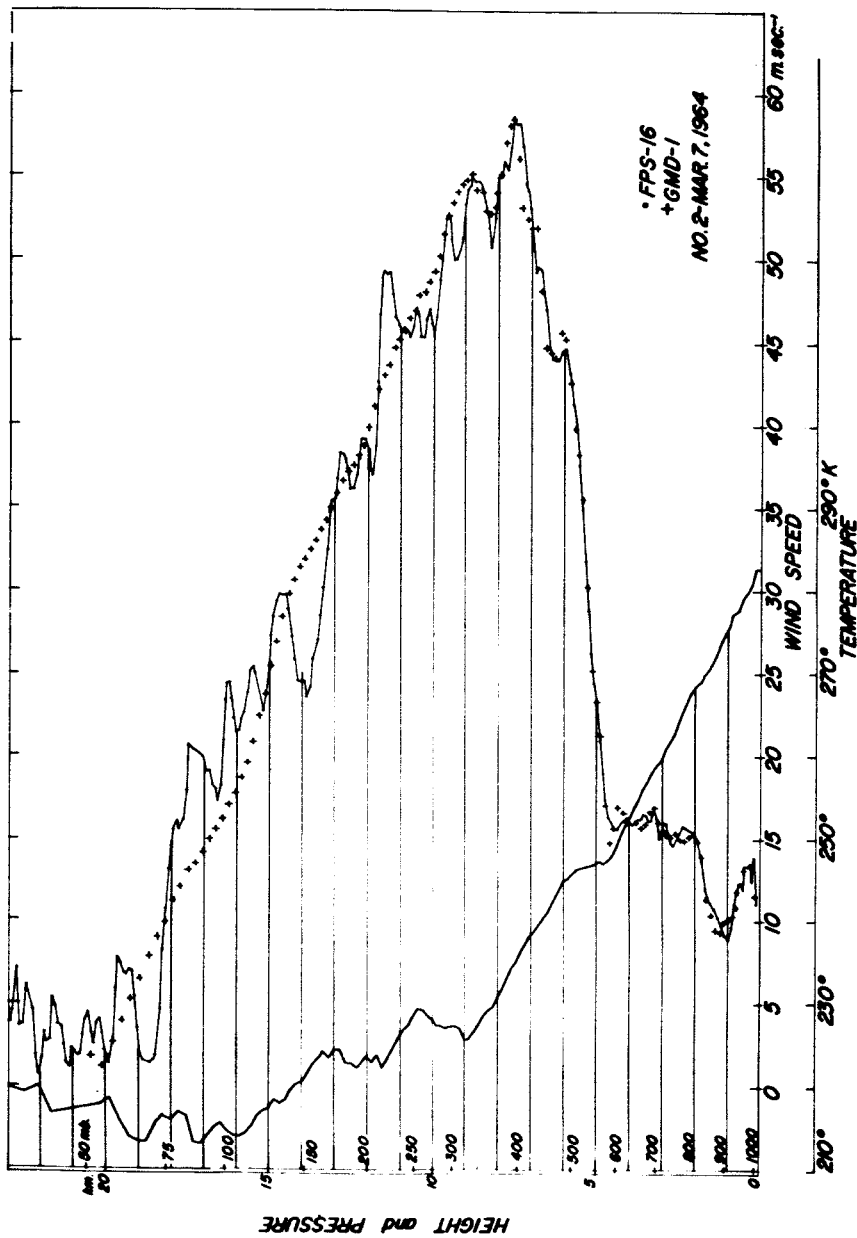


Figure 27: Wind speed and temperature profiles for 2nd ascent, March 7, 1964, (1107Z)

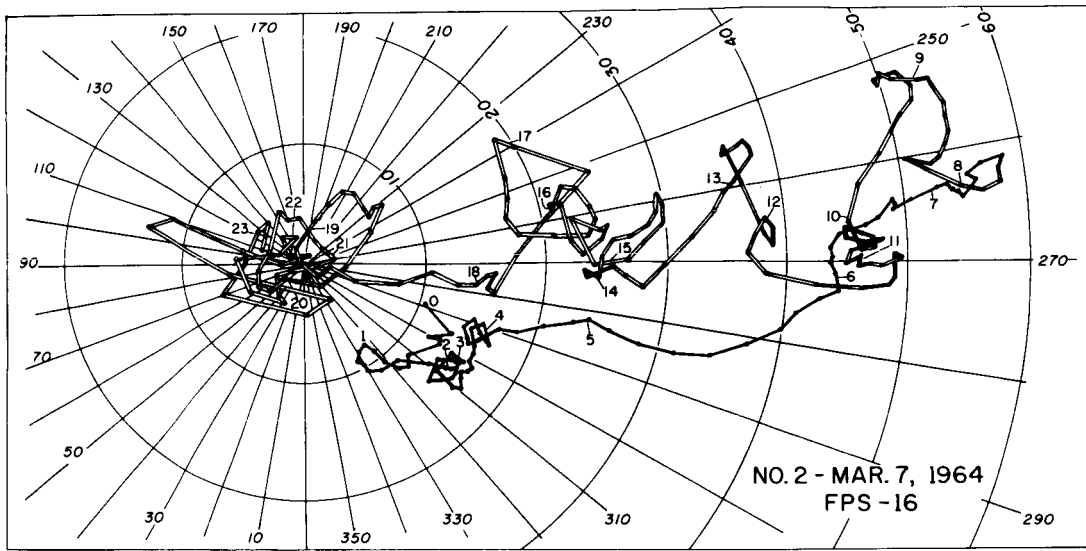


Figure 28: FPS-16 hodograph, 2nd ascent, March 7, 1964

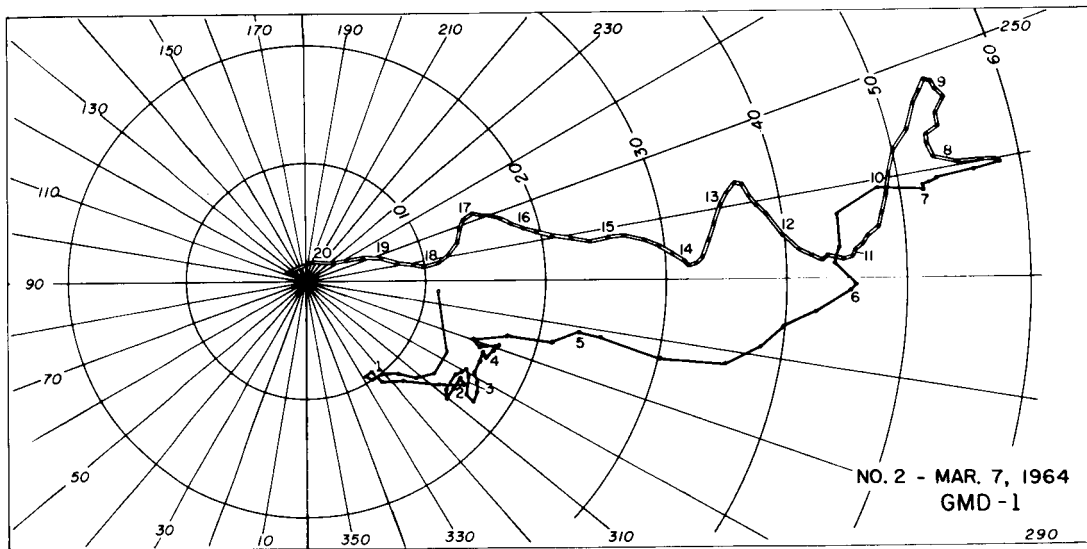


Figure 29: GMD-1 hodograph, 2nd ascent, March 7, 1964



wind speed is probably close to 8 km because the peak at 10.5 km is produced by a mesoscale oscillation superimposed on the mean. The superimposition can be clearly seen in Figure 25, where between 9.5 and 11.5 km, the FPS-16 hodograph forms almost a perfect circle. The circle could be reproduced by a 10 m/sec perturbation vector rotating anticyclonically with height. None of the loops in this or the other four FPS-16 hodographs were comparable in magnitude. Also, the temperature perturbations were 180 deg out of phase with the speed perturbations while in most of the other loops the phase angles were close to 90 deg.

The GMD hodograph, Figure 29, was calm and serene compared to the active oscillations in the FPS-16. As noted earlier in Figure 23, the portion derived from the polynomial passed through the loops in the FPS-16 hodograph. Therefore, the polynomial method appears to have produced a close approximation to the mean wind directions and speeds.

#### 9B. Second Ascent of March 7, 1964

At the time of the second ascent, 1107 GMT, the jet had descended to 7.5 km but the speed, 58 m/sec, was the same as the mean speed of the first ascent. In the speed profile, presented in Figure 27, a systematic error of 0.65 deg was subtracted from all the GMD elevation angles. As in the first ascent, the one contact averaging interval reproduced the FPS-16 speeds up to 8 km. Above this level, the curvature criterion was violated and a fourth order polynomial was fitted. The resulting winds deviated 2-4 m/sec from the mean of the FPS-16 winds between 13 and 18 km. At all other levels, the speeds were quite close to the mean.

The large amplitude mesoscale oscillations in wind speed and direction which produce the loop in Figure 25 is not evident in the speed profile but large angular turning is still evident in the hodograph, Figure 28. Between 9 and 13 km, the temperature perturbations are also 180 deg out of phase with the wind speed perturbations as they were twelve hours earlier.

In the final comparison, the GMD winds, Figure 29, contain all the dominant features of the hodograph up to 14 km. The multiple loops above 14 km are all smoothed out but the mean winds are again closely approximated.

## SECTION 10. EVIDENCE OF GRAVITY AND GRAVITY-INERTIAL WAVES

The hodographs of winds computed from the precision radar tracking data contain many mesoscale and microscale oscillations in wind speed and direction. If the hodographs are decomposed into mean velocities and vector deviations from the mean, the deviation vectors have magnitudes from 1 to 5 m/sec and change their direction with height. In most cases, the deviation vectors rotate anticyclonically with height. The combination of shears in the mean wind and the rotating vector produce the undulations and loops observed in the hodographs.

The order of magnitude of the perturbations in wind speed and temperature plus the small vertical wave lengths are consistent with the properties of gravity waves in an isothermal atmosphere at rest (Hines 1960, Eckhart 1960). However, the u and v perturbations of a gravity wave are linearly polarized while in the examples shown the larger perturbation vectors rotate with height.

Approximate perturbation solutions for shear-gravity and inertial-gravity waves will be presented in a following report. The solutions show that waves of both classes have rotating perturbation wind vectors similar to those found in the FPS-16 hodographs.

The magnitude of the curvature criterion, introduced in Section 5B, was determined by reference to the curvatures associated with these rotating perturbation vectors. In the five cases analyzed in this report, the curvature between three successive GMD winds was less than 4 m/sec when the GMD winds closely approximated the FPS-16 winds. Also, when the GMD elevation angles contained large errors, curvatures which greatly exceeded the criterion were frequently encountered. However, if the errors in elevation angles were organized over a long period, the curvature criterion might not be exceeded. It may be necessary to also include a criterion based on the magnitude of the vector deviations from the mean. The problem of separating the mesoscale oscillations from oscillations produced by errors in measurements deserves further study. It is worth noting that the curvature criterion is effective for detecting an error in one position coordinate. The curvatures at the two adjacent points are then of the opposite sign. A microscale oscillation could produce the same effect but their curvatures were again less than 4 m/sec in the cases studied.

## SECTION 11. CONCLUSIONS

The GMD-1 tracking and radiosonde data have been shown, by comparison to precision FPS-16 radar tracking data, to be sufficiently accurate to resolve both the macroscale and mesoscale features of the wind when: the angles are measured ten times the normal rate; the data is carefully read and then processed by machine; and the elevation angles are greater than 10 deg above the effective horizon.

At lower elevation angles, the errors in the elevation angles increase to 10 and 15 times the generally accepted RMS error. This increase is presumably due to the instruments inability to discriminate between direct and ground reflected or refracted signals. The combination of larger errors which contain long period fluctuations and the increased sensitivity to errors at low elevation angles precludes resolution of the mesoscale features of the winds.

To resolve the mean or macroscale features of the wind vectors as a function of height, the elevation angles were greatly smoothed by fitting a fourth order polynomial to several hundred consecutive observations. The limits of the curve fitting were determined by applying a curvature criterion to the wind vectors computed from position coordinates which were previously computed from averages of height, elevation and azimuth angles over one and three pressure contact intervals. The order of the polynomial was determined by comparing the reduction in the RMS error as the order of the Gram-Schmidt orthogonal polynomials was increased. In the five cases tested, the RMS error remained almost constant between the fourth and tenth order polynomials.

The winds computed from the FPS-16 measurements contain, between the earth's surface and the maximum altitude reached by the radiosonde balloon, many oscillations in wind speed and direction. The hodographs suggest that the velocities can be decomposed into a mean wind vector and a perturbation vector which rotates cyclonically or anticyclonically with height. In the stratosphere anticyclonic rotation predominates. The perturbation vectors have magnitudes ranging from 0.5 to 10 m/sec and rotate through  $2\pi$  radians in 0.5 to 3 km. The source of the perturbations remains unsolved but the properties of the vector wind and temperature perturbations are consistent with those of both inertial-gravity and shear-gravity waves.

APPENDIX  
Computer Programs

BEGIN DAFT SOURCE DECK  
PROGRAM TO PROCESS GMD DATA

JUNE 1965 R T DUQUET PENNA STATE UNIV DEPT OF METEO  
DECEMBER 1965 REVISION TO CURVE FIT

LIST OF SUBPROGRAMS USED WITH THIS PROGRAM

\*\*\*\*\*

METEANGLE AN ARCTAN ROUTINE  
WITH DIRECTION IN METEOROLOGICAL CONVENTION

WIND COMPUTES WIND SPEED AND DIRECTION (AND SHEAR  
GRADIENT) USING FINITE DIFFERENCES BETWEEN  
GEOMETRIC LOCATIONS BASED ON MEAN VALUES OF  
AZIMUTH AN ELEVATION ANGLES

SCAN A ROUTINE TO DETECT AND WARN OF POSSIBLE GROSS  
ERRORS IN INPUT VALUES

INTRPOLATE OBTAINS (1) WIND SPEED AND DIRECTION BY  
INTERPOLATION BETWEEN ADJACENT WIND VALUES  
AND (2) NEW WIND SHEAR GRADIENTS

CHARCMP AN "IF" STATEMENT TO COMPARE TWO STRINGS OF  
ALPHA CHARACTERS

LIST OF PRINCIPLE VARIABLE NAMES USED IN THIS PROGRAM

\*\*\*\*\*

A INPUT VALUES OF AZIMUTH ANGLE

ASCRT BALLOON ASCENT RATE (M/SEC)

AU MIXING RATIO

AZ AVERAGE VALUE OF AZIMUTH ANGLE  
(GMD TO BALLOON MEASURED FROM NORTH)

D HORIZONTAL DISTANCE OF BALLOON FROM OBSERVING GMD

DIR WIND DIRECTION (METEOROLOGICAL CONVENTION)

E INPUT VALUES OF ELEVATION ANGLE

EL AVERAGE VALUE OF ELEVATION ANGLE

ERRBASE LOWEST POINT CURRENTLY VIOLATING SHEAR CRITERION

ERRTOP HIGHEST POINT CURRENTLY VIOLATING SHEAR CRITERION  
(WITHIN A GIVEN DISTANCE OF OTHER VIOLATIONS)

ES SATURATION VAPOR PRESSURE

IC CONTACT NUMBER - USED TO CONTROL DATA ORDER

## APPENDIX (CONT'D)

INTERVAL	NUMBER OF ADDITIONAL PRESSURE CONTACT INTERVALS ON EACH SIDE OF CENTER FOR LONG AVERAGE WINDS
LASTPOINT	HIGHEST LEVEL NUMBER FOR THERMODYNAMIC DATA
LASTSHEAR	HIGHEST LEVEL NUMBER AT WHICH SHEAR GRADIENT CAN BE COMPUTED
LASTWIND	HIGHEST LEVEL NUMBER AT WHICH WIND CAN BE COMPUTED
MESSAGE	A SINGLE ALPHA CHARACTER USED TO FLAG WIND VALUES AT LEVELS WHICH REQUIRED SPECIAL TREATMENT
NP	NUMBER OF PRESSURE CONTACTS
NW	NUMBER OF AZIMUTH AND ELEVATION ANGLE DATA POINTS
P	PRESSURE AT A GIVEN CONTACT (MB)
R	RELATIVE HUMIDITY (PERCENT)
SHEARGRAD	WIND SHEAR GRADIENT BETWEEN SUCCESSIVE CONTACTS
SHEARLIMIT	AN ARBITRARY LIMIT ON THE SHEAR GRADIENT BETWEEN SUCCESSIVE LEVELS
SPD	WIND SPEED (CM/SEC)
T	TEMPERATURE AT PRESSURE CONTACT (ALSO USED FOR VIRTUAL TEMPERATURE)
TBAR	AVERAGE TIME ASCRIBED TO CONTACT MIDPOINT
TEMP	A TEMPORARY STORAGE ARRAY
TP	TIME OF PRESSURE CONTACT (MINUTES FROM RELEASE)
TW	TIME OF AZIMUTH AND ELEVATION ANGLE OBSERVATIONS
Z	HEIGHT OF BALLOON ABOVE STATION (METERS)
ZBAR	AVERAGE 'Z' ASCRIBED TO CONTACT MIDPOINT
ZS	HEIGHT OF STATION ABOVE M.S.L. (METERS)

## APPENDIX (CONT'D)

```

      INTEGER FIRSTAVERG, FIRSTWIND, FIRSTSHEAR, ERBASE, ERRTOP, UNIT
      CHARACTER LABEL(60), MESSAGE(150), CONTROL(10)
      COMMON A( 900), E( 900), TW( 900), TEMP( 900), AZ(150), EL(150),
1         D(150), X(150), Y(150), DIR(150), SPD(150), TP(150),
2         VW, LASTPOINT
      DIMENSION TBAR(150), ZBAR(150), Z(150), XN(150), SHEARGRAD(150),
1         JTOP(150)
      EQUIVALENCE (TEMP(1), TBAR), (TEMP(151), ZBAR), (TEMP(301), Z),
1         (TEMP(451), XN), (TEMP(601), SHEARGRAD), (TEMP(751), JTOP)
      DIMENSION P(150), T(150), R(150), ASCRT(150), IC(150)

C
      KEYPLOT = 1
      KOUNTFILES = 0
      REWIND 11
      READ FMT8, CONTROL, SHEARLIMIT
      CALL CHARCOMP(CONTROL(6), 'PLOT', 4, NOSET, SET, NOSET)
      KEYPLOT = 2
      IF( SHEARLIMIT) 2, 1, 2
1     SHEARLIMIT=4.0
      TAPE
2     CALL CHARCOMP(CONTROL, 'TAPE', 4, CARDS, TAPE, CARDS )
      UNIT = 14
      CALL TAPEMOUNT(14, 'METED 42 ', 1)
      CALL TAPECHECK
      GO TO START
      CARDS
      START
      UNIT = 70
      READ (UNIT, FMT1) LABEL, ZS
      CALL CHARCOMP(LABEL, 'END', 3, GO, STOP, GO)
      GO
      PRINT FMT0, LABEL
      DO 10 I=1, 150
10     MESSAGE(I)=' '

C
C     ***** READ THERMODYNAMIC DATA *****
C
      READDATA
      DO 33 I = 1, 150
      NP = I
      READ (UNIT, FMT3) IC(I), IP(I), P(I), T(I), IT, R(I)
      IF(TP(I) - 999.9) 30, 34, 30
30     IF(IT) 31, 32, 31
31     T(I) = 273.2-T(I)
      GO TO 33
32     T(I)=273.2+T(I)
33     CONTINUE
34     NNP = NP - 2
      NP = NP - 1
      LASTPOINT=NP
      LASTWIND = LASTPOINT - 1
      LASTSHEAR = LASTWIND - 1

C
C     CHECK FOR CORRECT ORDER
C
      KEY=0
      DO 39 I=2, NNP
      IF(IC(I+1)-IC(I)-1) 38, 35, 38
35     IF(TP(I+1)-TP(I)) 38, 38, 30
36     IF(P(I+1)-P(I)) 39, 38, 38
38     PRINT ERRMESAG, IC(I)
      KEY=1
39     CONTINUE
      IF(KEY) STDP, 40, STOP

```

## APPENDIX (CONT'D)

```

C
C      SMOOTH PRESSURE VERSUS CONTACT CURVE
C
40  TEMP(2) = P(2)
    TEMP(NP) = P(NP)
    DO 42  J = 1,2
    DO 41  I = 3, NNP
41  TEMP(I) = (P(I-1) + P(I) + P(I+1)) / 3.0
    DO 42  I = 3, NNP
42  P(I) = (TEMP(I-1) + TEMP(I) + TEMP(I+1)) / 3.0
C
C      SMOOTH TIME FUNCTION
C
    DO 43  I = 3, NNP
43  TEMP(I) = (TP(I) + TP(I+1) + TP(I-1)) / 3.0
    TEMP(2) = TP(2)
    TEMP(NP) = TP(NP)
    DO 44  I = 2, NNP
44  TP(I) = (TEMP(I) + TEMP(I+1) + TEMP(I-1)) / 3.0
C
C ***** READ WIND DATA *****
C
    DO 50 I=1,900
    NW = I
    READ (UNIT, FMT4) TW(I), e(I), A(I)
    IF(TW(I) - 999.9)50, 51, 50
50  CONTINUE
51  NW = NW - 1
C
C      CHECK FOR CORRECT ORDER
C
    KEY = 0
    DO 55  I = 2, NW
    IF(TW(I-1) - TW(I))55, 54, 54
54  KEY = 1
    PRINT FMT7, TW(I)
55  CONTINUE
    IF(KEY) STOP, 60, STOP
C
C      CHECK RAW WIND DATA FOR REASONABLE SMOOTHNESS
C
60  CALL SCAN(E, NW, 'ELEV')
    CALL SCAN(A, NW, 'AZIM')
    DO 62  I=1,NW
    A(I)=A(I)/57.296
62  E(I)=E(I)/57.296
C
C ***** OBTAIN HEIGHT FROM HYPSDMETRIC EQUATION *****
C
HEIGHT DO 72  I = 1, LASTPOINT
    ES = ((273.2/T(I))**5.2)*6.105*EXP (25.0*(1.0-(273.2/T(I))))
    AU=(0.622*ES / (P(I)-.378*ES))*R(I)
72  T(I) = T(I)*(1.0+.61*AU)
    Z(I)=0.0
    DO 75  I = 2, LASTPOINT
75  Z(I)=Z(I-1)+.287E7/980.6*(((T(I-1)*P(I)**.296-T(I)*P(I-1)**.286)/
1  (P(I)**.286-P(I-1)**.286))*ALOG(P(I-1)/P(I))-(T(I)-T(I-1))/.286)
    DO 77  I=2,LASTWIND
77  ASCRT(I)=(Z(I+1)-Z(I-1))/(TP(I+1)-TP(I-1))*1.667E-4

```

## APPENDIX (CONT'D)

```

C ***** OBTAIN WIND FROM AVERAGE OF AZIMUTH AND ELEVATION ANGLES *****
C
C CALL WIND(3, LASTWIND, 0)
C
C SCAN WIND FOR IMPROBABLE SHEAR GRADIENT
C
INTERVAL = 0
DO 1000 I = 4, LASTSHEAR
IF(ABS(SHEARGRAD(I))-SHEARLIMIT) 1000,1000,BADSPJT
ERRBASE=I
MESSAGE(I)='S'
KOUNT=0
ERRTOP=I
IF(ERRTOP-LASTSHEAR) 100,1000,1000
100 J=ERRTOP+1
K=ERRTOP+4
IF(K - LASTSHEAR) 101, 101, 200
101 DO 103 L=J,K
IF(ABS(SHEARGRAD(L))-SHEARLIMIT) 103,103,102
102 KOUNT=KOUNT+1+L-J
MESSAGE(L)='S'
ERRTOP=L
GO TO 100
103 CONTINUE
104 IF(KOUNT) 109,109,110
109 MESSAGE(I)='1'
GO TO 1000

C
C INTERPOLATE IF LARGE SHEAR GRADIENTS ARE FOUND IN SMALL SEGMENT
C
110 IF(INTERVAL) 111,111,LONGAVERG
111 IF(ERRTOP-(I+4)) 112,112,LONGAVERG
112 IF(KOUNT-2) 120,114,120
114 IF(SHEARGRAD(I)*SHEARGRAD(I+2)) 115,LONGAVERG,LDNGAVERG
115 CALL INTRPOLATE(I,1)
CALL INTRPOLATE(I+2,1)
MESSAGE(I)='E'
MESSAGE(I+2)='E'
GO TO TEST
120 IF(KOUNT-8) LONGAVERG,121,LONGAVERG
121 IF(SHEARGRAD(I+1)*SHEARGRAD(I+3)) 122,LDNGAVERG,LDNGAVERG
122 CALL INTRPOLATE(I+1,1)
CALL INTRPOLATE(I+3,1)
MESSAGE(I+1)='E'
MESSAGE(I+3)='E'
CALL INTRPOLATE(I,2)
CALL INTRPOLATE(I+2,2)
CALL INTRPOLATE(I+4,2)
GO TO TEST

```



## APPENDIX (CONT'D)

```

C
C      USE A LONGER AVERAGING PERIOD FOR SCATTERED SHEAR 'ERRORS'
C
      200  ERRTOP = LASTWIND
LONGAVERG  INTERVAL = INTERVAL + 1
            IF(INTERVAL-2) 201,202,202
      201  CALL WIND(ERRBASE, ERRTOP, INTERVAL)
            GO TO TEST
      202  DO FLAG, IJL=FRRBASE, ERRTOP
FLAG        MESSAGE(IJL)='X'
            CALL CURVEFIT(ERRBASE-10, ERRTOP+10)
            CALL WIND(ERRBASE-5, ERRTOP+5, 2)
            GO TO TEST
      1000 INTERVAL = 0
C
C ***** PRINT RESULTS *****
C
PRINT      PRINT FMT2, LABEL, SHEARLIMIT
            DO 9999 I = 1, LASTPOINT
            Z(I)=Z(I)/100.+ZS
            ZBAR(I)=ZBAR(I)/100.
            D(I)=D(I)/1.0E5
            N=XN(I)
            DIR(I)=DIR(I)*57.296
            AZ(I)=AZ(I)*57.296
            EL(I)=EL(I)*57.296
            PRINT FMT5, TBAR(I), ZBAR(I), AZ(I), FL(I), D(I), N, DIR(I),
1            SPD(I), MESSAGE(I)
      9999  PRINT FMT6, TP(I), P(I), I(I), Z(I), ASCRT(I)
            GO TO (START, WRITETAPE), KEYPLOT
WRITETAPE  WRITE(11) TBAR, ZBAR, AZ, EL, D, XN, DIR, SPD, MESSAGE, TP, P, T,
1          Z, ASCRT, LASTPOINT, LABEL
            KOUNTFILES = KOUNTFILES + 1
            GO TO START
STOP      IF(KOUNTFILES) CALL, END, CALL
CALL      WRITE(11) KOUNTFILES
            ENDFILE 11
            REWIND 11
            CALL SEGLDR(12, 'PLOT ')
END      STOP
C
FMT0      FORMAT('1 PROGRAM GMD-3 VERSION 001 '/'0',60C)
FMT1      FORMAT(60C,2F10.0)
FMT2      FORMAT(1H1, 60C, 5X,
1          'SHEARLIMIT = ',F5.1,/1H0/
2          /1H0, 4HTIME, 6X4HPRES, 5X5HVTEMP, 4X6HHEIG4T,
3          5X5HASCRT, 6X4HTBAR, 6X4HZBAR, 3X2HAZ, 8X2HEL, 5X4HDIST,
4          4X1HN, 7X3HDIR, 7X3HSPD ,2X4HNOTE, /
5          1H0, 4HMIN,8X2HMB,7X3HDEG,9X1HM,5X5HM/SEC,7X3HMIV,9X1HM,2BX2HKM,
6          20X5HM/SEC/1H0)
FMT3      FORMAT(110, 2F10.0, F9.1, 11, F10.2)
FMT4      FORMAT(F10.1, 2F10.2)
FMT5      FORMAT(1H0, 44X, 5F10.2, 15, 2F10.2 ,5X1C)
FMT6      FORMAT(1H0,F5.1,F9.1,3F10.2,5X,7C(1H*))
FMT7      FORMAT('0 WIND DATA NOT ORDERED AT TIME',F10.2)
FMT8      FORMAT(10C, F10.0)
ERRMESAG  FORMAT('0 DATA NOT ORDERED AT CONTACT NUMBER ',15)
E ND DAFT SO U RCE DECK

```

## APPENDIX (CONT'D)

```

SOURCE DECK
SUBROUTINE WIND(START, STOP, INTERVAL)
INTEGER START, STOP

COMMON A( 900), E( 900), TW( 900), TEMP( 900), AZ(150), EL(150),
1      D(150), X(150), Y(150), DIR(150), SPD(150), TP(150),
2      NW, LASTPOINT
DIMENSION TBAR(150), ZBAR(150), Z(150), XN(150), SHEARGRAD(150),
1      JTOP(150)
EQUIVALENCE (TEMP(1), TBAR), (TEMP(151), ZBAR), (TEMP(301), Z),
1      (TEMP(451), XN), (TEMP(601), SHEARGRAD), (TEMP(751), JTOP)

RE=.6371229 E 9
LIMIT3=START
LIMIT4=STOP
KEY=1
IF(START-(3+INTERVAL)) 1,2,2
1  LIMIT3=3+INTERVAL
KEY=2
2  IF(STOP-(LASTPOINT-INTERVAL-1)) 4,4,3
3  LIMIT4=LASTPOINT-INTERVAL-1
KEY=3
4  LIMIT1=LIMIT3-1
   LIMIT2=LIMIT4+1

GET MEAN HEIGHT AND TIME

DO 5  I = LIMIT1, LIMIT2
TBAR(I) = (TP(I-1-INTERVAL) + TP(I+INTERVAL)) / 2.0
5  ZBAR(I) = (Z(I-1-INTERVAL) + Z(I+INTERVAL)) / 2.0

AVERAGE AZIMUTH AND ELEVATION BETWEEN CONTACTS

DO 20  I = LIMIT1, LIMIT2
SUMA = 0.0
SUME = 0.0
XN(I)=0.
DO 15  J= 1, NW
IF( TW(J) - TP(I-1-INTERVAL)) 15, 10, 10
10 IF(TW(J) - TP(I+INTERVAL))11, 11, 14
11 JTOP(I)=J
SUMA = SUMA+A(J)
SUME = SUME + E(J)
XN(I)=XN(I)+1.0
15 CONTINUE
14 IF(XN(I)) 16, 18, 16
16 AZ(I) = SUMA/XN(I)
   EL(I) = SUME/XN(I)
GO TO 20
18 AZ(I) = 0.0
   EL(I) = 0.0
   JTOP(I)=NW
20 CONTINUE

```

## APPENDIX (CONT'D)

```

C
C
C
DISTANCE      DO 23  I = LIMIT1, LIMIT2
               XXX=COS (EL(I))/(1.+ZBAR(I)/RE)
               D(I) = RE * (1.5708 - ASIN(XXX) - EL(I))
               X(I)=D(I)*SIN (AZ(I))
23            Y(I) = D(I) * COS(AZ(I))

C
C
C
               OBTAIN WIND AND SHEAR GRADIENT BETWEEN CONTACTS (M/SEC)

               DO 90 I=LIMIT3,LIMIT4
               IP=I+INTERVAL
               IM=I-INTERVAL
               IF(JTOP(IP)-NW) 84,83,83
83            LIMIT6=I
               GO TO 150
84            U3=(X(IP)-X(IM))/(TBAR(IP)-TBAR(IM))
               V3=(Y(IP)-Y(IM))/(TBAR(IP)-TBAR(IM))
               SPD(I) = 1.667E-04 * SQRT(U3 ** 2 + V3 ** 2)
               CALL METEDANGLE(DIR(I),U3,V3)
               IF( I - (LIMIT3+ 2) ) 86, 85, 85
85            SHEARGRAD(I-1) = SQRT((U1 + U3 - 2.0 * U2) ** 2 + (V1 + V3 - 2.0 *
1            V2) **2 ) * 1.667E-04*SIGN(1.0,SPD(I)+SPD(I-2)-2.0*SPD(I-1))
86            U1=U2
               U2 = U3
               V1=V2
90            V2 = V3
91            CALL INTRPOLATE(LIMIT3,2)
               CALL INTRPOLATE(LIMIT4,2)
               GO TO (RETURN,ZEROLOW,ZERUHI),KEY
ZEROLOW       LIMIT5=START-1
               DO 100 I=1,LIMIT5
               SPD(I)=0.0
               DIR(I)=0.0
100           SHEARGRAD(I+1)=0.0
               RETURN
ZERUHI        LIMIT6=LIMIT4+1
150           DO 200 I=LIMIT6,LASTPOINT
               SPD(I)=0.0
               DIR(I)=0.0
200           SHEARGRAD(I-1)=0.0
RETURN        RETURN
E ND DAFT SO U RCE DECK

```

## APPENDIX (CONT'D)

```

B EGIN DAFT S DURCE DECK
  SUBROUTINE INTRPOLATE(I,NN)
  COMMON A( 900), E( 900), TW( 900), TEMP( 900), AZ(150), EL(150),
1     D(150), X(150), Y(150), DIR(150), SPD(150), TP(150),
2     NW, LASTPOINT
  DIMENSION SHEARGRAD(150)
  EQUIVALENCE (TEMP(601),SHEARGRAD)
  U1=SPD(I-1)*SIN(DIR(I-1)+3.1415927)
  V1=SPD(I-1)*COS(DIR(I-1)+3.1415927)
  U2=SPD(I+1)*SIN(DIR(I+1)+3.1415927)
  V2=SPD(I+1)*COS(DIR(I+1)+3.1415927)
  GO TO (1,2),NNN
1  U=(U1+U2)/2.
   V=(V1+V2)/2.
   SPD(I)=SQRT(U**2+V**2)
   CALL METEDANGLE(DIR(I),U,V)
   SHEARGRAD(I)=0.
   RETURN
2  U=SPD(I)*SIN(DIR(I)+3.1415927)
   V=SPD(I)*COS(DIR(I)+3.1415927)
   SHEARGRAD(I)=SQRT((U1+U2-2.*U)**2+(V1+V2-2.*V)**2)*
1     SIGN(1.0,SPD(I-1)+SPD(I+1)-2.0*SPD(I))
   RETURN
E ND DAFT SO U RCE DECK

```

```

B EGIN DAFT S DURCE DECK
  SUBROUTINE SCAN(W, N, NAME)
  CHARACTER NAME(4)
  COMMON A( 900), E( 900), TW( 900), TEMP( 900), AZ(150), EL(150),
1     D(150), X(150), Y(150), DIR(150), SPD(150), TP(150),
2     NW, LASTPOINT
  DIMENSION W(1000)
  DO 1  I = 2, N
1  TEMP(I) = W(I) - W(I-1)
   NL = 2
2  NI = NL
   NL = NL + 10
   IF( NL - N) 3, 3, RETURN
3  SUM = 0.0
   SUMSQ = 0.0
   DO 4  I = NI, NL
   SUM = SUM + TEMP(I)
4  SUMSQ = SUMSQ + TEMP(I) * TEMP(I)
   SUM = SUM / 11.0
   SUMSQ = SUMSQ / 11.0
   IF(SUMSQ - SUM * SUM) 2,2,OK
   STD = SQRT(SUMSQ - SUM * SUM)
   DO 6  I = NI, NL
   IF(ABS(TEMP(I)-SUM)-3.0*STD) 6,6,5
5  PRINT FMT1,NAME,W(I),TW(I)
6  CONTINUE
   GO TO 2
  RETURN
  FMT1  FORMAT('0',4C,' ANGLE HAS THE QUESTIONABLE VALUE',1PE11.3,
1     ' AT TIME',3PF8.2)
E ND DAFT SO U RCE DECK

```

## APPENDIX (CONT'D)

```
BEGIN DAFT SOURCE DECK
SUBROUTINE METEANGLE(D,U,V)
  IF(V) 10,11,10
  11 IF(U) 12,13,14
  12 D=1.5707963
  RETURN
  13 D=0.
  RETURN
  14 D=4.712389
  RETURN
  10 B=ATAN (ABS (U/V))
  IF(U) 1000,700,700
  700 IF(V) 800,1300,900
  800 D=6.2831853-B
  RETURN
  900 D=B+3.1415927
  RETURN
  1000 IF(V) 1100,1300,1200
  1100 D=B
  RETURN
  1200 D=3.1415927-B
  1300 RETURN
END DAFT SOURCE DECK
```

## APPENDIX (CONT'D)

```

B EGIN DAFT S OURCE DECK
SUBROUTINE CURVEFIT(III,JJJ)
COMMON A( 900), E( 900), TW( 900), TEMP( 900), AZ(150), EL(150),
1   D(150), X(150), Y(150), DIR(150), SPD(150), TP(150),
2   NW, LASTPOINT
REAL AAA(5)
II=III
JJ=JJJ
IF(II) 1,1,2
1   II=1
2   IF(JJ-LASTPOINT) 41,41,3
3   JJ=LASTPOINT
41  DO 5 I=1,NW
   IF(TP(II)-TW(I)) 4,4,5
4   ISTART=I-10
   GO TO 6
5   CONTINUE
   CALL STOPDUMP('CURVEFIT 1')
6   DO 10 I=1,NW
   JK=NW+1-I
   IF(TP(JJ)-TW(JK)) 10,7,7
7   IEND=JK+10
   GO TO 11
10  CONTINUE
   CALL STOPDUMP('CURVEFIT 2')
11  IF(ISTART) 12,12,13
12  ISTART=1
13  IF(IEND-NW) 15,15,14
14  IEND=NW
15  NNN=IEND-ISTART
   DO 50 I=1,5
   IO=I-1
   SUM=0.0
   PSUM=0.0
   DO 45 J=ISTART,IEND
   S=J-ISTART
   XX = GRAM(IO,S,NNN)
   SUM = SUM+XX*E(J)
45  PSUM = PSUM+XX*XX
50  AAA(I)=SUM/PSUM
   DO 70 J=ISTART,IEND
   S=J-ISTART
   XX=0.0
   DO 60 I=1,5
   IO=I-1
60  XX = XX + AAA(I)*GRAM(IO,S,NNN)
70  E(J)=XX
   RETURN
E ND DAFT SO U RCE DECK

```

## APPENDIX (CONT'D)

```

B EGIN DAFT S OURCE DECK
      FUNCTION GRAM(IR,S,N)
      IF(IR) ERR,ZERO,MORE
      CALL STOPDUMP('NEGGRAMARG')
      ERR
      ZERO      GRAM=1.0
                RETURN
      MORE      IF(MOD(IR,2)) ODD,EVEN,ODD
      ODD       CRN=-1.0
                GO TO 1
      EVEN      CRN=1.0
                1  R=IR
                  XN=N
                  C=1.0
                  SUM=1.0
                  FACT=1.0
                  IRP1=IR+1
                  TERM=1.0
                  T1=R+1.0
                  T1A=R
                  T2=S
                  T4=XN
                  DO LOOP,JK=2,IRP1
                  C=-C
                  K=JK-1
                  XK=K
                  FACT=FACT*XK
                  TERM=TERM*T1*T1A*T2/T4
                  T1=R+1.0+XK
                  T1A=R-XK
                  T2=S-XK
                  T4=XN-XK
      LOOP      SUM=C*TERM/(FACT*FACT)+SUM
                GRAM=SUM*CRN
                RETURN
E ND DAFT SO U RCE DECK

```

## REFERENCES

- Barbe, G.D., 1958: Donnes sur le vent en altitude., J. Sci. Met. 10, 47.
- Danielsen, E.F., 1959: The Laminar Structure of the Atmosphere and Its Relation to the Concept of a Tropopause., Arch. Met. Geoph. Biokl. AII. 3, 292-332.
- Eckart, C.H., 1960: Hydrodynamics of Oceans and Atmospheres (Pergamon, Oxford and New York).
- Forsythe, G.D., 1957: Generation and Use of Orthogonal Polynomials for Data-Fitting with a Digital Computer., J. Soc. Inc. Appl. Math., 5, 74-88.
- Hines, C.O., 1960: Internal Atmospheric Gravity Waves at Ionospheric Heights (Canadian J. of Phys., 28, 1441 - 1481).
- Sawyer, J.S., 1961: Quasi-Periodic Wind Variations with Height in the Lower Stratosphere., 87, 24-33.
- Scoggins, J.R., 1963: An Evaluation of Detailed Wind Data that is Measured by the FPS-16 Radar/Spherical Balloon Technique.  
NASA Technical Note TN D-1572, 30 pp.  
(S.T.A.R. # N63-15692, OTS: \$1.00).
- Scoggins, J.R., 1965: Spherical Balloon Wind Sensor Behavior J. Appl. Meteor., 4, 139-145.



## ACKNOWLEDGEMENTS

The authors are pleased to acknowledge the excellent cooperation of Orvel E. Smith, Chief of Terrestrial Environment Branch, NASA-MSFC., and the helpful assistance provided by graduate students, Young Bok Lee and W. John Hussey.

APPROVAL

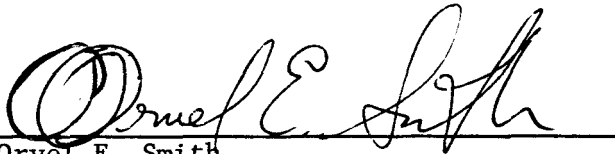
CR-61158

A COMPARISON OF FPS-16 AND GMD-1 MEASUREMENTS  
AND METHODS FOR PROCESSING WIND DATA

By E. F. Danielsen and R. T. Duquet

The information in this report has been reviewed for security classification. Review of any information concerning Department of Defense or Atomic Energy Commission programs has been made by the MSFC Security Classification Office. This report, in its entirety, has been determined to be unclassified.

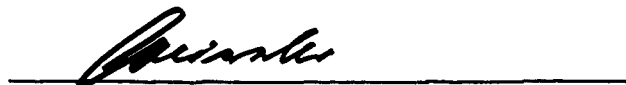
This document has also been reviewed and approved for technical accuracy.



Orvel E. Smith  
Chief, Terrestrial Environment Branch



William W. Vaughan  
Chief, Aerospace Environment Division



E. D. Geissler  
Director, Aero-Astrodynamic Laboratory

## DISTRIBUTION

## DEP-T

Dr. Rees

## R-DIR

Mr. Weidner  
Mr. Dannenberg

## R-AS-DIR

Mr. Williams

## R-EO-DIR

Dr. Johnson

## MS-IP

## MS-IPL (8)

## MS-H

## HME-P

## CC-P

## MS-T (5)

## R-AERO-X

Mr. Thoma

## R-AERO-DIR

Dr. Geissler  
Mr. Jean  
Mr. Clark

## R-AERO-A

Mr. Dahm  
Mr. Reed

## R-AERO-D

Mr. Horn (2)  
Mr. Rheinfurth (2)  
Mr. Ryan (2)  
Mr. Deaton (2)

## R-AERO-F

Mr. Lindberg  
Mr. Hill  
Mr. Stone  
Mr. Hagood

## R-AERO-G

Mr. Baker  
Mr. Blair  
Mr. Hart  
Mr. Schwaniger

## R-AERO-P

Mr. McNair

## R-AERO-T

Mr. Cummings  
Dr. Heybey  
Mr. Lavender  
Dr. Liu  
Mr. Murphree  
Mr. Jandebour

## R-AERO-Y

Mr. Dalton  
Mr. Daniels  
Mr. Dickey  
Mr. Kaufman  
Mr. Scoggins (2)  
Mr. O. Smith (25)  
Mr. R. Smith  
Mr. O. Vaughan  
Mr. W. Vaughan (2)  
Mr. Brown  
Mr. Sloan  
Mr. Falls  
Mr. Johnson  
Mr. R. Turner  
Mr. Camp  
Mr. Susko  
Mr. Hill

## DISTRIBUTION (CONT'D)

R-ASTR-DIR Dr. Haeussermann	Office of Advanced Research and Technology NASA Headquarters Washington, D. C. 20546 Attn: Mr. M. Ames      Dr. A. Kelley Mr. R. Rhode Mr. D. Gilstad Mr. R. E. Littell Dr. Jack Levine Mr. Douglas Michell Mr. Richard M. Bear
R-P&VE-DIR Dr. Lucas Mr. Hellebrand	
R-P&VE-P Mr. Paul	
R-P&VE-S Mr. Kroll Mr. R. Hunt	Office of Space Science and Applications NASA Headquarters Washington, D. C. 20546 Attn: Dr. Homer Newell Dr. John E. Naugle Dr. M. Tepper Mr. J. A. Salmanson Mr. W. Spreen
R-P&VE-V Mr. Aberg	
R-QUAL-DIR Mr. Grau	
R-TEST-DIR Mr. Heimburg	
R-TEST-T Dr. Reisig	NASA-Kennedy Space Flight Center Cocoa Beach, Florida 32931 Attn: Dr. Bruns, INS-1 Dr. Knothe, TEC Col. Petrone, PPR Mr. A. Taiani, PPR-72 Technical Library Lt. Col. R. L. Clark, SOP Mr. J. Deese, EDV-23
R-TEST-I Dr. Sieber Mr. B. Blake Mr. H. Rutledge	
RSIC Library (2)	
<u>EXTERNAL</u>	NASA-Langley Research Center Langley Field, Virginia 23365 Attn: Dr. F. L. Thompson, Director Mr. R. Hord Mr. T. Coleman Mr. Homer Morgan Mr. W. H. Reed, III Mr. V. Alley Mr. H. B. Tolefson Mr. I. E. Garrick Library (2)
Director Office of Manned Space Flight NASA Headquarters Washington, D. C. 20546 Attn: Dr. George Mueller, Director Mr. Phil Bolger	

## DISTRIBUTION (CONT'D)

NASA-Goddard Space Flight Center Greenbelt, Maryland 20771 Attn: Dr. W. Nordberg Mr. W. Spencer Library (2)	Commander Air Force Systems Command Andrews Air Force Base Washington, D. C. 20331
NASA-Flight Research Center Edwards Air Force Base, California 93523 Attn: Mr. Tom Toll	Mr. Kenneth Nagler Environmental Science Services Administration U. S. Weather Bureau Washington, D. C. 20235
Jet Propulsion Laboratory California Institute of Technology 4800 Oak Grove Drive Pasadena 3, California 91103 Attn: Technical Library	Office of Staff Meteorologist AFSC (SCWTS) Andrews Air Force Base Washington, D. C. 20331
NASA-Lewis Research Center 21000 Brookpark Road Cleveland, Ohio 44135 Attn: Mr. H. W. Plohr (Code: 9430) Mr. C. Wentworth (Code: 9310) Library	Air Force Systems Command (2) Space Systems Division Air Force Unit Post Office Los Angeles 45, California 90045 Meteorological & Geostrophysical Abstracts P. O. Box 1736 Washington 13, D. C. 20013
NASA-Ames Research Center Moffett Field Mountain View, California 94035 Attn: Dr. S. DeFrance, Director Library	Dr. Walter Boccus (2) Lockheed Missiles & Space Corporation Sunnyvale, California 94000
NASA-Manned Spacecraft Center Houston, Texas 77001 Attn: Technical Library (2) Mr. John P. Mayer Mr. Robert F. Thompson	Office of Scientific and Technical Information (25) Attn: NASA Representative (S-AK/RKT) P. O. Box 33 College Park, Maryland 20740
Mr. William Elam (2) Bellcomm, Inc. 1100 17th Street, NW Washington, D. C. 20036	Air Force Cambridge Research Laboratories Bedford, Massachusetts 01730 Attn: CRFL, Dr. J. S. Salisbury Technical Library (5)
Commander Headquarters, Air Weather Service Scott Air Force Base, Illinois 62225 Attn: Dr. Robert D. Fletcher Library (2)	Michoud Operations George C. Marshall Space Flight Center P. O. Box 26078 I-MICH-D New Orleans, Louisiana 70126

## DISTRIBUTION (CONT'D)

Member, MWG  
Inter-Range Instrumentation Group  
Attn: Major Vick  
APGC (PGGW)  
Eglin Air Force Base, Florida 32542

Member, MWG  
Inter-Range Instrumentation Group  
Attn: Lt. Colonel H. R. Montague (3)  
AFETR  
Patrick Air Force Base, Florida 32925

Dr. O. Essenwanger  
AMSMI-RRA, Bldg. 5429  
U. S. Army Missile Command  
Redstone Arsenal, Alabama

Member, MWG  
Inter-Range Instrumentation Group  
Attn: Mr. Orville Daniel  
PAWA/GMRD, AFMTC,  
MU-235, Technical Library  
Patrick Air Force Base, Florida 32925

Member, MWG  
Inter-Range Instrumentation Group  
Attn: Lt. Col. I. Van Blunt  
AFFTC (FTZBW)  
Edwards Air Force Base, California  
93523

Member, MWG  
Inter-Range Instrumentation Group  
Attn: Mr. Royal C. Gould  
Code 3069  
Naval Ordnance Test Station  
China Lake, California 93557

Member, MWG  
Inter-Range Instrumentation Group  
Attn: Mr. Tom Carr  
Code 3150 (2)  
Comdr. Summerville,  
Code 3250, Box 22 (2)  
Pacific Missile Range  
Point Mugu, California 93041

Member, MWG  
Inter-Range Instrumentation Group  
Attn: Mr. Willis L. Webb (3)  
SELWS-M, USAERDA  
White Sands Missile Range,  
New Mexico 88002

Associated Member, MWG  
Inter-Range Instrumentation Group  
Attn: Mr. Robert Leviton  
AFCRL (CRER), OAR  
1065 Main Street  
Waltham, Massachusetts 02154

Associated Member, MWG  
Inter-Range Instrumentation Group  
Attn: Mr. V. S. Hardin  
AWSSS/TRSD  
Air Weather Service  
Scott Air Force Base, Illinois

Associated Member, MWG  
Inter-Range Instrumentation Group  
Attn: Mr. Kenneth Steelmen  
AMSEL-RD-SM  
USAERDL  
Fort Monmouth, New Jersey

Associate Member, MWG  
Inter-Range Instrumentation Group  
Attn: Mr. A. Lewis Miller  
Meteorological Management Division  
Bureau of Naval Weapons  
Washington 25, D. C.

Associate Member, MWG  
Inter-Range Instrumentation Group  
Attn: Mr. John F. Spurling  
NASA-Wallops Station  
Wallops Island, Virginia 23337

## DISTRIBUTION (CONT'D)

Associate Member, MWG  
 Inter-Range Instrumentation Group  
 Attn: Mr. Vaughn D. Rockney  
 DATAC Division  
 U. S. Weather Bureau  
 24th and M Streets, N.W.  
 Washington 25, D. C.

Associated Member, MWG  
 Inter-Range Instrumentation Group  
 Attn: Mr. Clifford A. Olson  
 Code 7261  
 Sandia Corporation  
 Sandia Base  
 Albuquerque, New Mexico 87110

Dr. Jack L. Hough  
 Department of Meteorology and  
 Oceanography  
 University of Michigan  
 Ann Arbor, Michigan 48105

Commander  
 Air Force Flight Dynamics Laboratory  
 Air Force Systems Command  
 Wright-Patterson AFB, Ohio 45433  
 Attn: Mr. Thomas D. Lemley  
 Mr. George Muller

Aerospace Corporation  
 P. O. Box 95081  
 El Segundo, California 90245  
 Attn: Dr. Henry G. Maier

Dr. Edwin F. Danielsen (15)  
 The Pennsylvania State University  
 Department of Meteorology  
 College of Mineral Industries  
 University Park, Pennsylvania 16802

Mr. H. C. S. Thom  
 Environmental Data Service  
 Gramax Building  
 Room 724  
 8060 13th Street, N.W.  
 Silver Springs, Maryland 20910

Dr. Harold L. Crutcher  
 National Weather Records Center  
 Federal Building  
 Asheville, North Carolina 28801

Dr. A. C. Cohen, Jr.  
 Department of Statistics  
 University of Georgia  
 Athens, Georgia 30601

Dr. C. E. Buell  
 Kaman Nuclear  
 Garden of the Gods Road  
 Colorado Springs, Colorado 80907

Dr. Ghomas Gleeson  
 Professor of Meteorology  
 Department of Meteorology  
 Florida State University  
 Tallahassee, Florida 32306

Professor Noel LaSuer  
 Department of Meteorology  
 Florida State University  
 Tallahassee, Florida 32306

Professor C. Jordan  
 Department of Meteorology  
 Florida State University  
 Tallahassee, Florida 32306

Dr. Gerald L. Barger  
 Environmental Data Service  
 Gramax Building, Room 730  
 8060 13th Street, N. W.  
 Silver Springs, Maryland 20910

The Boeing Company  
 New Orleans, Louisiana  
 Attn: Mr. Wayne R. Covington

Dr. Arnold Court  
 17168 Septo Street  
 Northridge, California 91324

## DISTRIBUTION (CONT'D)

Dr. Sidney Teweles  
U. S. Weather Bureau  
Washington, D. C. 20331

Mr. Norman Sissenwine (2)  
Air Force Cambridge Research Laboratories  
Code: CREW

L. G. Hanscom Field  
Bedford, Massachusetts

Mr. Jack Reed  
Sandia Corporation  
Albuquerque, New Mexico

Mr. Edmund Blond  
Manager, Special Studies  
Aerospace Corporation  
2350 E. El Segundo Blvd.  
El Segundo, California 90245

Mr. Thomas Y. Palmer  
Research Specialist  
Aerospace Division  
Boeing Company  
MS 23-81 656-PS88  
P. O. Box 3707  
Seattle, Washington

Professor Elmar R. Reiter  
Department of Atmospheric Science  
Colorado State University  
Fort Collins, Colorado 80521

Mr. Marvin Diamond  
U. S. Army Electronics R&D Activity  
Attn: Environmental Sciences Department  
White Sands Missile Range, New Mexico 88002

Director  
Meteorological Division  
U. S. Army Signal Research & Development Laboratories  
Fort Monmouth, New Jersey

Mr. John C. Mester  
U. S. Army Ballistics Research  
Laboratories

Attn: AMXBR-B  
Aberdeen Proving Ground, Maryland  
21005

U. S. Army Electronics Research and  
Development Activity  
Fort Huachuca, Arizona 86513  
Attn: Mr. A. V. Carlson, SELHU-M (2)  
Meteorology Department  
Library (2)

Commanding Officer (2)  
United States Army  
Frankford Arsenal  
Attn: Mr. David Askin, Q6200  
Building 230  
Philadelphia, Pennsylvania 19137